Formation-Containment Control Using Dynamic Event-Triggering Mechanism for Multi-Agent Systems

Amir Amini, *Student Member, IEEE*, Amir Asif, *Senior Member, IEEE*, and Arash Mohammadi, *Senior Member, IEEE*

***Abstract*—The paper proposes a novel approach for formation-containment control based on a dynamic event-triggering mechanism for multi-agent systems. The leader-leader and follower-follower communications are reduced by utilizing the distributed dynamic event-triggered framework. We consider two separate sets of design parameters: one set comprising control and dynamic event-triggering parameters for the leaders and a second set similar to the first one with different values for the followers. The proposed algorithm includes two novel stages of co-design optimization to simultaneously compute the two sets of parameters. The design optimizations are convex and use the weighted sum approach to enable a structured trade-off between the formation-containment convergence rate and associated communications. Simulations based on non-holonomic mobile robot multi-agent systems quantify the effectiveness of the proposed approach.**

***Index Terms*—Co-design convex optimization, dynamic event-triggered schemes, formation-containment control, multi-agent systems.**

I. Introduction

COOPERATIVE behaviours have attracted considerable attention in a variety of multi-agent system (MAS) applications, including leaderless consensus [1], leader-following consensus [2], [3], containment control [4]–[7], and formation control [8], [9]. Recently, the formation-containment control (FCC) framework, which can be regarded as the combined problem of formation and containment for multi-agent systems, has arisen in several engineering applications [10]–[20]. In FCC, the leaders converge to a desired geometric formation. Simultaneously, the followers merge within the convex hull spanned by the leaders. As compared to solitary containment [4]–[7] and solitary formation [8], [9], FCC is more complex and a topic of increasing interest in the control and signal processing community. A related application for FCC is the mixed containment-sensing problem [21] where the objective is to have a group of mobile agents (followers) cover and provide surveillance sequentially from one region of interest to another. In this application, the leaders steer the followers from one operational region (formation) to another and coordinate the sensing task for the followers. This paper considers the FCC problem for general linear multi-agent systems using a comprehensive event-triggering scheme, usually known as the dynamic event-triggering mechanism.

Formation-containment has been studied for agents with different dynamics, including second-order linear agents [10], [11], general linear agents [12]–[14], heterogeneous agents [15], [16], Euler–Lagrange systems [17], [18], and a class of nonlinear agents [19]. All of these implementations impose the strict condition of real-time data transmissions between the agents. To preserve the limited energy allocated to each agent, event-triggered mechanisms [22]–[28] that reduce communications are of great interest in FCC applications.

The implementation of an event-triggered scheme often requires a design step for computing parameters associated with the control protocol and event-triggering scheme. In many event-triggered implementations used in cooperative control of networked systems, control gains are either assumed as *a priori* information [22]–[24] or designed as a separate step based on the Hurwitz stability of the closed-loop systems [25], [26]. In such emulation-based approaches, the design of event-triggering thresholds is based on a pre-selected value for the control gain. The operational regions obtained for the event-triggered parameters are, therefore, conditioned on the control gains and may not be the best choices. Alternatively, the control gain and event-triggering parameters are designed simultaneously through a unified optimization framework. In this co-design approach, all parameters are computed together based on a predefined objective, such as H_∞ optimization [27] or inter-event interval maximization [28].

As one of the most advanced event-triggered schemes, *dynamic* event-triggered mechanism (DEM) have recently been proposed in [29]–[31]. In DEM, an internal dynamic

Manuscript received January 23, 2020; revised March 25, 2020; accepted April 13, 2020. This work was partially supported by the Natural Sciences and Engineering Research Council (NSERC) of Canada through the NSERC Discovery (RGPIN-2016-04988). Recommended by Associate Editor Giuseppe Franzè. *(Corresponding author: Arash Mohammadi.)*

Citation: A. Amini, A. Asif, and A. Mohammadi, "Formation-containment control using dynamic event-triggering mechanism for multi-agent systems," *IEEE/CAA J. Autom. Sinica*, vol. 7, no. 5, pp. 1235–1248, Sept. 2020.

A. Amini and A. Asif are with the Electrical and Computer Engineering, Concordia University, Montreal, Quebec H3G 2W1, Canada (e-mail: amir.amini@mail.concordia.ca; amir.asif@concordia.ca).

A. Mohammadi is with the Concordia Institute for Information System Engineering, Concordia University, Montreal, Quebec H3G 1M8, Canada (e-mail: arash.mohammadi@concordia.ca).

Color versions of one or more of the figures in this paper are available online at http://ieeexplore.ieee.org.

Digital Object Identifier 10.1109/JAS.2020.1003288

variable is included as an additional threshold to the event-triggering parameters. One interesting feature of the DEMs is that their inter-event interval can be longer than the so-called static event-triggered schemes. At the same time, the desired cooperative objectives (such as formation and containment) can still be reached using DEM without introducing steady-state errors. This is in contrast to some other implementations [32] where the event-triggered scheme reduces the number of transmissions at the expense of a bounded error for the desired cooperative behaviour.

Motivated by the aforementioned limitations in the existing FCC approaches, the paper proposes a formation-containment control approach using a dynamic event-triggered mechanism (FCC/DEME) that offers optimality for design parameters, namely the control gains and event-triggering parameters. The main features of the proposed FCC/DEME are listed below:

1) To the best of our knowledge, FCC/DEME is the first implementation for formation-containment that utilizes the *dynamic* event-triggered mechanism. This leads to considerable energy and communication savings for the multi-agent systems.

2) Two different sets of control and *dynamic* event-triggering parameters are introduced for: i) formation of the leaders; and ii) containment of the followers. To design these parameters, FCC/DEME utilizes two convex optimizations based on enabling a trade-off between the rate of convergence for formation-containment and the frequency of the events.

3) The design approaches [30], [31], derive some bounded regions for the DEM design parameters. It should be noted that even when the regions for design parameters are known, selecting the operating values that efficiently save transmissions is still difficult and requires some trial and error. Instead, in FCC/DEME the co-design optimization computes the exact values of the design parameters based on one proposed objective function.

Perhaps, the closest work to FCC/DEME is [20], where an event-triggered formation-containment implementation is proposed. Unlike [20], the DEM used in this paper is more general and adds additional degrees of freedom. As another difference, FCC/DEME (unlike [20]) is based on an optimization framework to develop a structured trade-off between the formation-containment convergence rate and frequency of the transmissions.

The remaining paper is organized as follows. Section II introduces notation and preliminary concepts. Section III formulates the formation-containment problem. Section IV develops two unified optimizations (one for the leaders and one for the followers) for parameter design. Simulation examples are included in Section V. Finally, Section VI concludes the paper.

II. Preliminaries

We use alphabets in bold fonts for matrices and vectors. Scalars are denoted by alphabets in normal font. $\|\cdot\|$: L_2 norm; $(\cdot)^{\dagger}$: Pseudo inverse; $\boldsymbol{A}>0$: Matrix $\boldsymbol{A}$ is symmetric positive definite; 1: Column vector with all entries equal to 1; $\boldsymbol{I}$: Identity matrix; $\boldsymbol{0}$: Zero matrix; $\otimes$: Kronecker product; $*$: Transpose of the corresponding block matrix.

A. Multi-Agent System

Consider the following general linear MAS:

$$\dot{\boldsymbol{x}}_i(t)=\boldsymbol{A}\boldsymbol{x}_i(t)+\boldsymbol{B}\boldsymbol{u}_i(t),\quad i\in\mathcal{V}=\{1,\ldots,N+M\} \tag{1}$$

where $\boldsymbol{x}_i(t)\in\mathbb{R}^n$ and $\boldsymbol{u}_i(t)\in\mathbb{R}^m$ are respectively the state and control input for agent i. Matrix pair $(\boldsymbol{A},\boldsymbol{B})$ is controllable.

There exist two sets of agents in MAS (1), namely, the followers and leaders. The follower and leader sets are, respectively, denoted by $\mathcal{F}=\{i\in\mathcal{V}\,|\,1\le i\le N\}$, and $\mathcal{L}=\{i\in\mathcal{V}\,|\,N+1\le i\le N+M\}$. For follower i $(1\le i\le N)$, we use notation $\mathcal{N}^i_{\mathcal{F}\leftarrow\mathcal{F}}$ to represent the set of its neighbours, which are also followers. The neighbours of follower i within the leaders' set are denoted by $\mathcal{N}^i_{\mathcal{F}\leftarrow\mathcal{L}}$. For leader i $(N+1\le i\le N+M)$, the set of its neighbours which are also leaders is denoted by $\mathcal{N}^i_{\mathcal{L}\leftarrow\mathcal{L}}$. Additionally, the neighbours of leader i within the followers' set is denoted by $\mathcal{N}^i_{\mathcal{L}\leftarrow\mathcal{F}}$.

Assumption 1: The follower-follower and leader-leader communication network topologies are connected and undirected. None of the leaders receive communication from the followers' set, i.e., $\mathcal{N}^i_{\mathcal{L}\leftarrow\mathcal{F}}$ is a null set for all leaders. In physical terms, the leaders are autonomous and are not restrained in their movement by the followers. There exists at least one directed path originating from one of the leaders to any follower in MAS (1).

Under Assumption 1, the associated Laplacian matrix $\boldsymbol{L}\in\mathbb{R}^{(N+M)\times(N+M)}$ with MAS (1) is given as follows:

$$\boldsymbol{L}=\begin{bmatrix}\boldsymbol{L}_{\mathcal{F}(N\times N)} & \boldsymbol{L}_{\mathcal{F}\mathcal{L}(N\times M)}\\ \boldsymbol{0} & \boldsymbol{L}_{\mathcal{L}(M\times M)}\end{bmatrix}. \tag{2}$$

Under Assumption 1, all eigenvalues of $\boldsymbol{L}_{\mathcal{F}}$ are positive real scalars. Each element in $-\boldsymbol{L}_{\mathcal{F}}^{-1}\boldsymbol{L}_{\mathcal{F}\mathcal{L}}$ is non-negative, and each row of $-\boldsymbol{L}_{\mathcal{F}}^{-1}\boldsymbol{L}_{\mathcal{F}\mathcal{L}}$ has a sum equal to one [4].

Illustrative Example: To illustrate the graph notation used in this paper, an example of a network with 10 agents (4 leaders, i.e., $M=4$, and 6 followers, i.e., $N=6$) is provided. This network is shown in Fig. 1. Based on Fig. 1, the neighbouring sets for agents 6 and 7, for example, are as follows: $\mathcal{N}^6_{\mathcal{F}\leftarrow\mathcal{F}}=\{1,5\}$, $\mathcal{N}^6_{\mathcal{F}\leftarrow\mathcal{L}}=\{8\}$, $\mathcal{N}^7_{\mathcal{L}\leftarrow\mathcal{L}}=\{8,10\}$, $\mathcal{N}^7_{\mathcal{L}\leftarrow\mathcal{F}}=\{\}$. The following blocks represent different partitions for the Laplacian matrix (2) corresponding to this network:

$$\boldsymbol{L}_{\mathcal{F}}\begin{bmatrix}2&0&0&-1&0&-1\\0&2&-1&-1&0&0\\0&-1&2&0&-1&0\\-1&-1&0&3&0&0\\0&0&-1&0&3&-1\\-1&0&0&0&-1&3\end{bmatrix}$$

$$\boldsymbol{L}_{\mathcal{L}}\begin{bmatrix}2&-1&0&-1\\-1&2&-1&0\\0&-1&2&-1\\-1&0&-1&2\end{bmatrix},\ \boldsymbol{L}_{\mathcal{F}\mathcal{L}}=\begin{bmatrix}0&0&0&0\\0&0&0&0\\0&0&0&0\\-1&0&0&0\\0&0&-1&0\\0&-1&0&0\end{bmatrix}. \tag{3}$$

Definition 1 (Formation): For a given formation vector $\boldsymbol{h}_i\in\mathbb{R}^n$, the leaders are said to achieve state formation if there exists a formation reference function $\boldsymbol{r}(t)\in\mathbb{R}^n$ such that

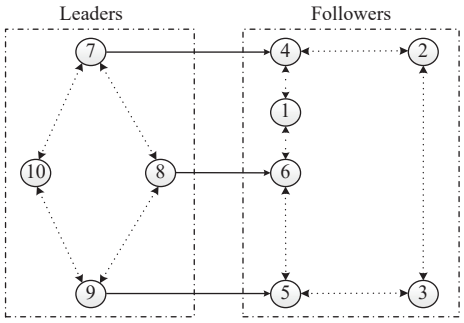

Fig. 1. An illustrative network topology.

$\lim_{t\to\infty}(\boldsymbol{x}_i(t)-\boldsymbol{h}_i-\boldsymbol{r}(t))=0$, $\forall i\in\mathcal{L}$, $\forall \boldsymbol{x}_i(0)\in\mathbb{R}^n$. As a result, it holds that $\lim_{t\to\infty}(\boldsymbol{x}_i(t)-\boldsymbol{x}_j(t))=\boldsymbol{h}_i-\boldsymbol{h}_j$, $\forall i,j\in\mathcal{L}$. In this paper, we consider constant (time-invariant) formation vector $\boldsymbol{h}_i$, $\forall i\in\mathcal{L}$.

We note that the leaders can determine the desired state formation by selecting proper values for formation vector $\boldsymbol{h}_i$, ($i\in\mathcal{L}$). According to Definition 1, when formation is achieved it holds that $\lim_{t\to\infty}(\boldsymbol{x}_i(t)-\boldsymbol{h}_i)=\lim_{t\to\infty}\boldsymbol{r}(t)$, $\forall i\in\mathcal{L}$. This implies that the disagreements between $\boldsymbol{x}_i(t)$ and its corresponding formation vector $\boldsymbol{h}_i$ approaches the reference function $\boldsymbol{r}(t)$ for all leaders. Fig. 2 is provided to show the relationships between $\boldsymbol{x}_i(t)$, $\boldsymbol{h}_i$, and $\boldsymbol{r}(t)$ for an illustrative formation for 3 leaders. From Fig. 2, we infer that the formation reference $\boldsymbol{r}(t)$ describes the macroscopic movement of the whole formation, and $\boldsymbol{h}_i$ is the relative offset between $\boldsymbol{x}_i(t)$ and $\boldsymbol{r}(t)$. As shown later in Remark 5, the reference function $\boldsymbol{r}(t)$ is dependent on the initial state of the leaders and formation vectors $\boldsymbol{h}_i$.

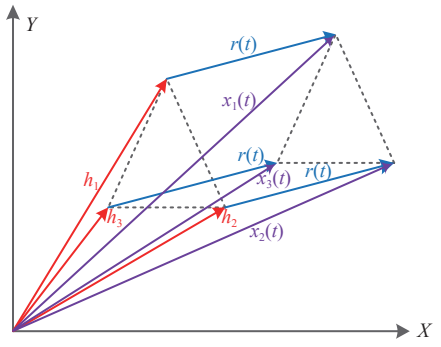

Fig. 2. An illustrative example for 3 leaders forming a triangle. When formation is achieved, it holds that $\lim_{t\to\infty}(\boldsymbol{x}_i(t)-\boldsymbol{h}_i-\boldsymbol{r}(t))=0$ ($1\le i\le 3$).

Definition 2 (Containment): Containment is said to be solved if starting from any initial states, the states of the followers converge to a convex hull formed by the leaders.

Definition 3 (Formation-Containment): MAS (1) is said to achieve formation-containment if for any initial values, the leaders converge to the desired formation and the followers achieve containment.

B. Dynamic Event-Triggering Scheme and Control Protocol

The agents share their states within their neighbourhoods to achieve formation-containment. To reduce the amount of transmission, an event-detector is incorporated with each agent. The event-detector in agent i (leader or follower) monitors a "dynamic event-triggering condition" to determine whether to transmit the state value $\boldsymbol{x}_i(t)$ within its neighbourhood. If the event detector detects an event at time instant $t^i_{k^{[i]}}$ (superscript i indicates agent i, and subscript $k^{[i]}=0,1,\ldots$ denotes the sequence of events for agent i), then agent i transmits $\boldsymbol{x}_i\left(t^i_{k^{[i]}}\right)$ to its neighbours. Upon receiving $\boldsymbol{x}_i\left(t^i_{k^{[i]}}\right)$, agent j (a neighbour of agent i), updates its previous database with the newly received state from agent i. This state value, i.e., $\boldsymbol{x}_i\left(t^i_{k^{[i]}}\right)$, is used at agent j until the next event is triggered by agent i. Let $\hat{\boldsymbol{x}}_i(t)\triangleq\boldsymbol{x}_i\left(t^i_{k^{[i]}}\right)$, $t\in\left[t^i_{k^{[i]}},t^i_{k^{[i]}+1}\right)$. We denote the following disagreement vectors, for followers and leaders:

$$\mathbb{X}_i(t)=\sum_{j\in\mathcal{N}^i_{\mathcal{L}\leftarrow\mathcal{L}}}\mathfrak{a}_{i,j}\left((\boldsymbol{\Lambda}_i(t)\hat{\boldsymbol{x}}_i(t)-\boldsymbol{h}_i)-(\boldsymbol{\Lambda}_j(t)\hat{\boldsymbol{x}}_j(t)-\boldsymbol{h}_j)\right),\ \forall i\in\mathcal{L} \tag{4}$$

$$\mathbb{X}_i(t)=\sum_{j\in\mathcal{N}^i_{\mathcal{F}\leftarrow\mathcal{F}}}\mathfrak{a}_{i,j}\left(\boldsymbol{\Lambda}_i(t)\hat{\boldsymbol{x}}_i(t)-\boldsymbol{\Lambda}_j(t)\hat{\boldsymbol{x}}_j(t)\right)-\sum_{j\in\mathcal{N}^i_{\mathcal{F}\leftarrow\mathcal{L}}}\mathfrak{a}_{i,j}\boldsymbol{x}_j(t),\ \forall i\in\mathcal{F} \tag{5}$$

where $\mathfrak{a}_{i,j}$ is element (i,j) in the weighted adjacency matrix and $\boldsymbol{\Lambda}_i(t)=e^{\boldsymbol{A}\left(t-t^i_{k^{[i]}}\right)}$. In Remark 2 (to be introduced later), we comment on $\boldsymbol{\Lambda}_i(t)$ and its impact on MAS (1).

Remark 1: Based on (4) and (5), the follower-follower and leader-leader state exchanges are event-triggered. Similar to [5], [6], [20], [26], the leader-to-follower transmission in FCC/DEME is continuous. Compared with the existing formation-containment implementations [10]–[13], [15]–[19] where all transmissions across the network are continuous, all in-neighbour transmissions in FCC/DEME except for the leader-to-follower communication are event-triggered. It should be noted that the leader-to-follower state transmission can be performed by a different subset of leaders during the formation-containment process (as shown later). This enhances the longevity of the leaders.

Let all agents transmit their initial state values $\boldsymbol{x}_i(0)$ to their neighbours, i.e., $t^i_0=0$, $\forall i\in\mathcal{F}\cup\mathcal{L}$. We denote the state error at time instant t by $\boldsymbol{e}_i(t)=\boldsymbol{\Lambda}_i(t)\hat{x}_i(t)-\boldsymbol{x}_i(t)$, $\forall i\in\mathcal{F}\cup\mathcal{L}$, Motivated by [30], the next event instant after $t^i_{k^{[i]}}$, $\forall i\in\mathcal{F}\cup\mathcal{L}$, is triggered based on the following dynamic event-triggering condition:

$$t^i_{k^{[i]}+1}=\inf\{t>t^i_{k^{[i]}}|\ \|\boldsymbol{\Phi}_c\boldsymbol{e}_i(t)\|\ge\alpha_c\|\mathbb{X}_i(t)\|+\beta_c\eta_i(t)\} \tag{6}$$

where $\boldsymbol{\Phi}_c\in\mathbb{R}^{n\times n}>0$, $\alpha_c>0$, and $\beta_c>0$ for $c\in\{1,2\}$ are design parameters. In (6), if $i\in\mathcal{L}$ then $c=1$ is used and if $i\in\mathcal{F}$ then $c=2$. Parameter $\eta_i(t)$ satisfies

$$\dot{\eta}_i(t)=-\gamma_c\eta_i(t)+\rho_c\|\mathbb{X}_i(t)\|,\quad \forall i\in\mathcal{V} \tag{7}$$

where $\eta_i(0)>0$. Parameters $\gamma_c>0$ and $\rho_c>0$ are to be designed. Similar to (6), in (7) if $i\in\mathcal{L}$ then $c=1$ and if $i\in\mathcal{F}$ then $c=2$.

The proposed distributed control protocol for the control

input is given below:

$$\boldsymbol{u}_i(t)=\begin{cases}\boldsymbol{K}_1\mathbb{X}_i(t)+\boldsymbol{H}\sum\limits_{j\in\mathcal{N}^i_{\mathcal{L}\leftarrow\mathcal{L}}}\mathfrak{a}_{i,j}(\boldsymbol{h}_i-\boldsymbol{h}_j), & i\in\mathcal{L}\\ \boldsymbol{K}_2\mathbb{X}_i(t), & i\in\mathcal{F}.\end{cases}\tag{8}$$

Matrices $\boldsymbol{K}_1\in\mathbb{R}^{m\times n}$ and $\boldsymbol{K}_2\in\mathbb{R}^{m\times n}$ are the control gains to be designed. Additionally, matrix $\boldsymbol{H}\in\mathbb{R}^{m\times n}$ is the formation gain which is also unknown and needs to be designed. As shown later in Remark 4, the term $\boldsymbol{H}\sum_{j\in\mathcal{N}^i_{\mathcal{L}\leftarrow\mathcal{L}}}\mathfrak{a}_{i,j}(\boldsymbol{h}_i-\boldsymbol{h}_j)$ is used in (8) to expand the set of possible formations that the leaders can achieve [9].

Remark 2 (State Estimation in Control Protocol): The proposed control protocol (8) benefits from an open loop estimate of the states in their event intervals [33]. More specifically, the expression $e^{\boldsymbol{A}(t-t^i_{k[i]})}\boldsymbol{x}_i(t^i_{k[i]})$ is an open-loop estimate of $\boldsymbol{x}_i(t)$ for $t^i_{k[i]}\le t\le t^i_{k[i]+1}$. Using the open-loop state estimation helps reduce the number of event-triggerings [34] as compared to other approaches where the events are triggered without any estimation.

Remark 3 (Special Cases for DEM (6)): We note that many existing event-triggered schemes can be regarded as special cases of (6). Under certain conditions, DEM (6) reduces to a number of widely used event-triggered schemes, including the followings:

i) If $\alpha_c=0$ and (7) is revised to $\dot\eta_i(t)=-\gamma_c\eta_i(t)$, then $\eta_i(t)=\eta_i(0)e^{-\gamma_c t}$. Therefore, DEM (6) reduces to

$$t^i_{k[i]+1}=\inf\{t>t^i_{k[i]}\mid\|\boldsymbol{\Phi}_c\boldsymbol{e}_i(t)\|\ge\beta_c\eta_i(0)e^{-\gamma_c t}\}.$$

ii) If $\alpha_c=0$ and $\dot\eta_i(t)=0$, then DEM (6) reduces to

$$t^i_{k[i]+1}=\inf\{t>t^i_{k[i]}\mid\|\boldsymbol{\Phi}_c\boldsymbol{e}_i(t)\|\ge\beta_c\eta_i(0)\}.$$

iii) If $\beta_c=0$, then threshold $\eta_i(t)$ is not involved in the event-triggering condition. Hence,

$$t^i_{k[i]+1}=\inf\{t>t^i_{k[i]}\mid\|\boldsymbol{\Phi}_c\boldsymbol{e}_i(t)\|\ge\alpha_c\|\mathbb{X}_i(t)\|\}.$$

The event-triggering schemes used in [35], [36] are a combination of the aforementioned items i) and ii). Additionally, combining ii) and iii) results in the event-triggering schemes used in [32], [37], [38].

C. Design Objectives

The design objectives in FCC/DEME are as follows:

1) Reduce the frequency of follower-follower and leader-leader state transmissions (event-triggerings).

2) Add flexibility to control the rate of formation-containment convergence rate.

3) Govern the potential trade-off between the formation-containment convergence rate and the frequency of event-triggerings.

4) Compute the exact values of unknown parameters in a co-design optimization framework based on an objective function which increases the inter-event interval.

III. Problem Formulation

In this section, we obtain the closed-loop MAS. Then, we convert the FCC problem into an equivalent stability problem. The co-design optimizations proposed in Section IV are based on stabilization of the converted systems.

A. Closed-Loop Multi-Agent System

We define the following global vectors:

$$\begin{aligned}&\boldsymbol{x}_{\mathcal{F}}=[\boldsymbol{x}_1^T(t),\dots,\boldsymbol{x}_N^T(t)]^T\quad\boldsymbol{x}_{\mathcal{L}}=[\boldsymbol{x}_{N+1}^T(t),\dots,\boldsymbol{x}_{N+M}^T(t)]^T\\&\hat{x}_{\mathcal{F}}=[\hat{\boldsymbol{x}}_1^T(t),\dots,\hat{\boldsymbol{x}}_N^T(t)]^T\quad\hat{x}_{\mathcal{L}}=[\hat{\boldsymbol{x}}_{N+1}^T(t),\dots,\hat{\boldsymbol{x}}_{N+M}^T(t)]^T\\&\boldsymbol{e}_{\mathcal{F}}=[\boldsymbol{e}_1^T(t),\dots,\boldsymbol{e}_N^T(t)]^T\quad\boldsymbol{e}_{\mathcal{L}}=[\boldsymbol{e}_{N+1}^T(t),\dots,\boldsymbol{e}_{N+M}^T(t)]^T\\&\boldsymbol{\eta}_{\mathcal{F}}=[\eta_1(t),\dots,\eta_N(t)]^T\quad\boldsymbol{\eta}_{\mathcal{L}}=[\eta_{N+1}(t),\dots,\eta_{N+M}(t)]^T\\&\mathbb{X}_{\mathcal{F}}=[\mathbb{X}_1^T(t),\dots,\mathbb{X}_N^T(t)]^T\ \mathbb{X}_{\mathcal{L}}=[\mathbb{X}_{N+1}^T(t),\dots,\mathbb{X}_{N+M}^T(t)]^T\\&\boldsymbol{\Lambda}_{\mathcal{F}}=\mathrm{diag}(\boldsymbol{\Lambda}_1(t),\dots,\boldsymbol{\Lambda}_N(t))\\&\boldsymbol{\Lambda}_{\mathcal{L}}=\mathrm{diag}(\boldsymbol{\Lambda}_{N+1}(t),\dots,\boldsymbol{\Lambda}_{N+M}(t))\\&\bar{\mathbb{X}}_{\mathcal{F}}=[\,\|\mathbb{X}_1(t)\|,\dots,\|\mathbb{X}_N(t)\|\,]^T\\&\bar{\mathbb{X}}_{\mathcal{L}}=[\,\|\mathbb{X}_{N+1}(t)\|,\dots,\|\mathbb{X}_{N+M}(t)\|\,]^T\\&\bar{\boldsymbol{e}}_{\mathcal{F}}=[\,\|\boldsymbol{e}_1(t)\|,\dots,\|\boldsymbol{e}_N(t)\|\,]^T\\&\bar{\boldsymbol{e}}_{\mathcal{L}}=[\,\|\boldsymbol{e}_{N+1}(t)\|,\dots,\|\boldsymbol{e}_{N+M}(t)\|\,]^T\\&\boldsymbol{h}=[\boldsymbol{h}_1,\dots,\boldsymbol{h}_M]^T.\end{aligned}\tag{9}$$

It holds that $\boldsymbol{e}_{\mathcal{L}}=\boldsymbol{\Lambda}_{\mathcal{L}}\hat{x}_{\mathcal{L}}-\boldsymbol{x}_{\mathcal{L}}$ and $\boldsymbol{e}_{\mathcal{F}}=\boldsymbol{\Lambda}_{\mathcal{F}}\hat{x}_{\mathcal{F}}-\boldsymbol{x}_{\mathcal{F}}$. The closed-loop system from (1) and (8) is given below:

$$\begin{aligned}\dot{\boldsymbol{x}}_{\mathcal{L}}=&(\boldsymbol{I}_M\otimes\boldsymbol{A}+\boldsymbol{L}_{\mathcal{L}}\otimes\boldsymbol{B}\boldsymbol{K}_1)\boldsymbol{x}_{\mathcal{L}}+\boldsymbol{L}_{\mathcal{L}}\otimes\boldsymbol{B}\boldsymbol{K}_1(\boldsymbol{e}_{\mathcal{L}}-\boldsymbol{h})\\&+(\boldsymbol{L}_{\mathcal{L}}\otimes\boldsymbol{B}\boldsymbol{H})\boldsymbol{h}\end{aligned}\tag{10}$$

$$\begin{aligned}\dot{\boldsymbol{x}}_{\mathcal{F}}=&(\boldsymbol{I}_N\otimes\boldsymbol{A}+\boldsymbol{L}_{\mathcal{F}}\otimes\boldsymbol{B}\boldsymbol{K}_2)\boldsymbol{x}_{\mathcal{F}}+\boldsymbol{L}_{\mathcal{F}}\otimes\boldsymbol{B}\boldsymbol{K}_2\boldsymbol{e}_{\mathcal{F}}\\&+\boldsymbol{L}_{\mathcal{F}\mathcal{L}}\otimes\boldsymbol{B}\boldsymbol{K}_2\boldsymbol{x}_{\mathcal{L}}.\end{aligned}\tag{11}$$

B. System Transformation

In this section, we convert the FCC problem for the original closed-loop MAS (10) and (11) into the stability problem for a transformed system. System transformation is accomplished in the following 3 steps.

Step 1: In the first step, we convert the problem of formation for the leaders into an equivalent stability problem. Let $\boldsymbol{z}=\boldsymbol{x}_{\mathcal{L}}-\boldsymbol{h}$. Based on $\boldsymbol{z}$, system (10) is expressed as

$$\begin{aligned}\dot{\boldsymbol{z}}=&(\boldsymbol{I}_M\otimes\boldsymbol{A}+\boldsymbol{L}_{\mathcal{L}}\otimes\boldsymbol{B}\boldsymbol{K}_1)\boldsymbol{z}+\boldsymbol{L}_{\mathcal{L}}\otimes\boldsymbol{B}\boldsymbol{K}_1\boldsymbol{e}_{\mathcal{L}}\\&+(\boldsymbol{I}_M\otimes\boldsymbol{A}+\boldsymbol{L}_{\mathcal{L}}\otimes\boldsymbol{B}\boldsymbol{H})\boldsymbol{h}.\end{aligned}\tag{12}$$

One widely-used approach to guarantee stability in (12) is to convert it into an equivalent system by eigenvalue decomposition of $\boldsymbol{L}_{\mathcal{L}}$. Let $0<\lambda_{2,\mathcal{L}}\le\cdots\le\lambda_{M,\mathcal{L}}$ denote the eigenvalues of $\boldsymbol{L}_{\mathcal{L}}$ in the ascending order. Let matrix $\boldsymbol{W}=[w_{i,j}]\in\mathbb{R}^{M\times M}$ include the normalized eigenvectors of $\boldsymbol{L}_{\mathcal{L}}$ such that

$$\boldsymbol{W}\boldsymbol{J}_1\boldsymbol{W}^{-1}=\boldsymbol{L}_{\mathcal{L}},\quad\|\boldsymbol{W}\|=1$$

where $\boldsymbol{J}_1=\mathrm{diag}(0,\lambda_{2,\mathcal{L}},\dots,\lambda_{M,\mathcal{L}})$ includes all eigenvalues of $\boldsymbol{L}_{\mathcal{L}}$. Let $\boldsymbol{W}^{-1}=[\tilde{w}_{i,j}]$. From $\boldsymbol{W}^{-1}$, we construct the $(M-1)\times M$ dimensional matrix $\tilde{\boldsymbol{W}}=[\tilde{w}_{i,j}]$, for $2\le i\le M$ and $1\le j\le M$. In other words, $\tilde{\boldsymbol{W}}$ includes rows 2 to M of matrix $\boldsymbol{W}^{-1}$. Now, we consider the following transformation:

$$\boldsymbol{\psi}_{\mathcal{L}}=\tilde{\boldsymbol{W}}\otimes\boldsymbol{I}_n\boldsymbol{z}.\tag{13}$$

Using (13), system (12) is transformed to

$$\begin{aligned}\dot{\boldsymbol{\psi}}_{\mathcal{L}}=&(\boldsymbol{I}_{M-1}\otimes\boldsymbol{A}+\tilde{\boldsymbol{J}}_1\otimes\boldsymbol{B}\boldsymbol{K}_1)\boldsymbol{\psi}_{\mathcal{L}}+\tilde{\boldsymbol{J}}_1\tilde{\boldsymbol{W}}\otimes\boldsymbol{B}\boldsymbol{K}_1\boldsymbol{e}_{\mathcal{L}}\\&+(\tilde{\boldsymbol{W}}\otimes\boldsymbol{A})\boldsymbol{h}+(\tilde{\boldsymbol{W}}\otimes\boldsymbol{I}_n)(\boldsymbol{L}_{\mathcal{L}}\otimes\boldsymbol{B}\boldsymbol{H})\boldsymbol{h}\end{aligned}\tag{14}$$

where $\tilde{\boldsymbol{J}}_1=\mathrm{diag}(\lambda_{2,\mathcal{L}},\dots,\lambda_{M,\mathcal{L}})$. In fact, $\boldsymbol{\psi}_{\mathcal{L}}$ is a disagreement

between the state of the leaders and their respective formation vectors. It is proved in [9, Theorem 1] that formation is achieved in (10) if and only if $\lim_{t\to\infty}\boldsymbol{\psi}_{\mathcal{L}}=0$. Similar to [9], [12]–[14], [16], [39], the term $(\tilde{\boldsymbol{W}}\otimes\boldsymbol{A})\boldsymbol{h}+(\tilde{\boldsymbol{W}}\otimes\boldsymbol{I}_n)(\boldsymbol{L}_{\mathcal{L}}\otimes\boldsymbol{BH})\boldsymbol{h}$ in (14) should be made zero to guarantee $\lim_{t\to\infty}\boldsymbol{\psi}_{\mathcal{L}}=0$. More precisely, the following condition, which is known as the formability condition, should be satisfied.

Formability Condition: For given formation vectors $\boldsymbol{h}_i$, ($i\in\mathcal{L}$), if there exists a formation gain $\boldsymbol{H}$ such that the following condition is satisfied:

$$(\boldsymbol{A}+\boldsymbol{BH})\sum_{j\in\mathcal{N}^i_{\mathcal{L}\leftarrow\mathcal{L}}}\mathfrak{a}_{i,j}(\boldsymbol{h}_i-\boldsymbol{h}_j)=\boldsymbol{0},\quad(\forall i\in\mathcal{L}) \tag{15}$$

then formation for leaders is feasible with respect to $\boldsymbol{h}_i$. For proof of (15), refer to [9, Theorem 2]. Under (15), (14) reduces to

$$\dot{\boldsymbol{\psi}}_{\mathcal{L}}=(\boldsymbol{I}_{M-1}\otimes\boldsymbol{A}+\tilde{\boldsymbol{J}}_1\otimes\boldsymbol{BK}_1)\boldsymbol{\psi}_{\mathcal{L}}+\tilde{\boldsymbol{J}}_1\tilde{\boldsymbol{W}}\otimes\boldsymbol{BK}_1\boldsymbol{e}_{\mathcal{L}}. \tag{16}$$

Step 2: Let

$$\boldsymbol{\psi}_{\mathcal{F}}=\boldsymbol{x}_{\mathcal{F}}+\left(\boldsymbol{L}_{\mathcal{F}}^{-1}\boldsymbol{L}_{\mathcal{FL}}\right)\otimes\boldsymbol{I}_n\boldsymbol{x}_{\mathcal{L}}. \tag{17}$$

If $\lim_{t\to\infty}\boldsymbol{\psi}_{\mathcal{F}}=0$, it holds that

$$\lim_{t\to\infty}\left[\boldsymbol{x}_{\mathcal{F}}+\left(\boldsymbol{L}_{\mathcal{F}}^{-1}\boldsymbol{L}_{\mathcal{FL}}\right)\otimes\boldsymbol{I}_n\boldsymbol{x}_{\mathcal{L}}\right]=0.$$

Since the row sum of $-\boldsymbol{L}_{\mathcal{F}}^{-1}\boldsymbol{L}_{\mathcal{FL}}$ equals one, the term $(\boldsymbol{L}_{\mathcal{F}}^{-1}\boldsymbol{L}_{\mathcal{FL}})\otimes\boldsymbol{I}_n\boldsymbol{x}_{\mathcal{L}}$ expresses a convex hull of the leaders' states to which $\boldsymbol{x}_{\mathcal{F}}$ converges. Therefore, containment is achieved in the sense of Definition 2 if $\lim_{t\to\infty}\boldsymbol{\psi}_{\mathcal{F}}=0$. Now, we transform (11) under transformation (17) and formability condition (15)

$$\begin{aligned}\dot{\boldsymbol{\psi}}_{\mathcal{F}}=&(\boldsymbol{I}_N\otimes\boldsymbol{A}+\boldsymbol{L}_{\mathcal{F}}\otimes\boldsymbol{BK}_2)\boldsymbol{\psi}_{\mathcal{F}}+\boldsymbol{L}_{\mathcal{F}}\otimes\boldsymbol{BK}_2\boldsymbol{e}_{\mathcal{F}}\\&+(\boldsymbol{I}_N\otimes\boldsymbol{BK}_1)(\boldsymbol{L}_{\mathcal{F}}^{-1}\boldsymbol{L}_{\mathcal{FL}}\boldsymbol{L}_{\mathcal{L}}\otimes\boldsymbol{I}_n)\boldsymbol{z}\\&+(\boldsymbol{I}_N\otimes\boldsymbol{BK}_1)(\boldsymbol{L}_{\mathcal{F}}^{-1}\boldsymbol{L}_{\mathcal{FL}}\boldsymbol{L}_{\mathcal{L}}\otimes\boldsymbol{I}_n)\boldsymbol{e}_{\mathcal{L}}.\end{aligned} \tag{18}$$

Step 3: If $\lim_{t\to\infty}\boldsymbol{\psi}_{\mathcal{L}}=0$, formation is achieved for the leaders with respect to Definition 1. As a result, it holds that $\lim_{t\to\infty}\boldsymbol{z}=\boldsymbol{x}_{\mathcal{L}}-\boldsymbol{h}=\boldsymbol{1}_M\otimes\boldsymbol{r}(t)$. Therefore, the third term on the right hand side of (18) approaches $(\boldsymbol{I}_N\otimes\boldsymbol{BK}_1)(\boldsymbol{L}_{\mathcal{F}}^{-1}\boldsymbol{L}_{\mathcal{FL}}\boldsymbol{L}_{\mathcal{L}}\otimes\boldsymbol{I}_n)\boldsymbol{1}_M\otimes\boldsymbol{r}(t)$. Since $\boldsymbol{L}_{\mathcal{L}}\boldsymbol{1}_M=\boldsymbol{0}$, it holds that

$$\lim_{t\to\infty}(\boldsymbol{I}_N\otimes\boldsymbol{BK}_1)(\boldsymbol{L}_{\mathcal{F}}^{-1}\boldsymbol{L}_{\mathcal{FL}}\boldsymbol{L}_{\mathcal{L}}\otimes\boldsymbol{I}_n)\boldsymbol{z}=\boldsymbol{0}. \tag{19}$$

The state error for leaders $\boldsymbol{e}_{\mathcal{L}}$ approaches zero, i.e., $\lim_{t\to\infty}\boldsymbol{e}_{\mathcal{L}}=0$. This fact together with (19) imply that the asymptotic stability for (18) can be simplified to the asymptotic stability of the following system:

$$\dot{\boldsymbol{\psi}}_{\mathcal{F}}=(\boldsymbol{I}_N\otimes\boldsymbol{A}+\boldsymbol{L}_{\mathcal{F}}\otimes\boldsymbol{BK}_2)\boldsymbol{\psi}_{\mathcal{F}}+\boldsymbol{L}_{\mathcal{F}}\otimes\boldsymbol{BK}_2\boldsymbol{e}_{\mathcal{F}}. \tag{20}$$

We use a similar eigenvalue decomposition for (20). Let matrix $\boldsymbol{V}$ be the normalized eigenvector matrix for $\boldsymbol{L}_{\mathcal{F}}$ such that

$$\boldsymbol{VJ}_2\boldsymbol{V}^{-1}=\boldsymbol{L}_{\mathcal{F}},\qquad\|\boldsymbol{V}\|=1 \tag{21}$$

where $\boldsymbol{J}_2=\mathrm{diag}(\lambda_{1,\mathcal{F}},\ldots,\lambda_{N,\mathcal{F}})$ includes all eigenvalues of $\boldsymbol{L}_{\mathcal{F}}$. We consider the following transformation:

$$\tilde{\boldsymbol{\psi}}_{\mathcal{F}}=\boldsymbol{V}^{-1}\otimes\boldsymbol{I}_n\boldsymbol{\psi}_{\mathcal{F}}. \tag{22}$$

Using (22), system (20) is transformed to

$$\dot{\tilde{\boldsymbol{\psi}}}_{\mathcal{F}}=(\boldsymbol{I}_N\otimes\boldsymbol{A}+\boldsymbol{J}_2\otimes\boldsymbol{BK}_2)\tilde{\boldsymbol{\psi}}_{\mathcal{F}}+(\boldsymbol{J}_2\boldsymbol{V}^{-1}\otimes\boldsymbol{BK}_2)\boldsymbol{e}_{\mathcal{F}}. \tag{23}$$

In conclusion, the formation-containment problem for MAS (1) is solved if systems (16) and (23) are stable.

We note that, unlike $\boldsymbol{L}_{\mathcal{L}}$, all eigenvalues of $\boldsymbol{L}_{\mathcal{F}}$ are strictly positive. Therefore, the transformation used in (22) is based on all eigenvectors included in $\boldsymbol{V}$. In contrast, in (13) we excluded the corresponding eigenvector to eigenvalue of zero.

Remark 4: According to the formability condition (15), linear MASs cannot achieve all the formation vectors due to the dynamic constraints of the agents. Similar observations for formability in general linear MASs have been made in other implementations including [9], [12]–[14], [16], [39]. The physical interpretation of (15) is that the expected formation should comply with the dynamics of the leaders [12]. We note that if $\boldsymbol{H}=\boldsymbol{0}$ in control protocol (8), the formability condition (15) reduces to $\boldsymbol{A}\sum_{j\in\mathcal{N}^i_{\mathcal{L}\leftarrow\mathcal{L}}}\mathfrak{a}_{i,j}(\boldsymbol{h}_i-\boldsymbol{h}_j)=\boldsymbol{0}$. Therefore, including the formation gain $\boldsymbol{H}$ expands the set of feasible formations that the leaders can achieve. It should be noted that for some formation vectors and agent dynamics, the formation gain $\boldsymbol{H}$ may be unnecessary (i.e., $\boldsymbol{H}$ can be zero). We will comment on this matter in Section V.

Remark 5: It is worth mentioning that if formation is achieved (i.e., $\lim_{t\to\infty}\boldsymbol{\psi}_{\mathcal{L}}=0$), the explicit expression for formation reference function $\boldsymbol{r}(t)$ satisfies

$$\lim_{t\to\infty}(\boldsymbol{r}(t)-\boldsymbol{r}_0(t)-\boldsymbol{r}_h(t))=0 \tag{24}$$

where

$$\begin{aligned}\boldsymbol{r}_0(t)&=e^{\boldsymbol{A}t}(\tilde{\boldsymbol{w}}_1\otimes\boldsymbol{I}_n)\boldsymbol{x}_{\mathcal{L}}(0)\\\boldsymbol{r}_h(t)&=-e^{\boldsymbol{A}t}(\tilde{\boldsymbol{w}}_1\otimes\boldsymbol{I}_n)\boldsymbol{h}\\&\quad+\int_0^t e^{\boldsymbol{A}(t-v)}((\tilde{\boldsymbol{w}}_1\otimes\boldsymbol{I}_n)(\boldsymbol{I}_M\otimes\boldsymbol{A}+\boldsymbol{L}_{\mathcal{L}}\boldsymbol{BH}))\boldsymbol{h}\,dv\end{aligned}$$

and $\tilde{\boldsymbol{w}}_1$ is row 1 of $\boldsymbol{W}^{-1}$. For proof of (24) refer to [9, Theorem 3]. Based on (24), the formation reference function $\boldsymbol{r}(t)$ depends on both the leaders' initial states $\boldsymbol{x}_{\mathcal{L}}(0)$ and global formation vector $\boldsymbol{h}$. In particular, $\boldsymbol{r}_0(t)$ is the impact of $\boldsymbol{x}_{\mathcal{L}}(0)$ on $\boldsymbol{r}(t)$, while $\boldsymbol{r}_h(t)$ shows how different choices of $\boldsymbol{h}_i$ impact $\boldsymbol{r}(t)$.

IV. Main Results

In this section, we first exclude the possibility of Zeno-behaviour for DEM (6) by obtaining a lower bound for the interval between two successive events. We explain how this lower bound relates the design objectives mentioned in Section II-C. Two separate optimizations are then developed to co-design unknown parameters. The first optimization simultaneously computes all design parameters ($\boldsymbol{K}_1$, $\boldsymbol{\Phi}_1$, α_1, β_1, γ_1, and ρ_1) for the leaders. The second optimization co-designs all design parameters ($\boldsymbol{K}_2$, $\boldsymbol{\Phi}_2$, α_2, β_2, γ_2, and ρ_2) for the followers.

A. Exclusion of Zeno-Behaviour

We begin this section with the following lemma which will be used for the exclusion of the Zeno-behaviour.

Lemma 1: It holds that $\eta_i(t)>\eta_i(0)e^{-(\gamma_c+\beta_c\frac{\rho_c}{\alpha_c})t}$, $\forall t\geq 0$, $\forall i\in\mathcal{V}$, and $c\in\{1,2\}$. Hence, $\eta_i(t)$ remains positive over time.

Proof: Based on (6), for $t\in[t^i_{k[i]},t^i_{k[i]+1})$, it holds that $\|\boldsymbol{\Phi}_c\boldsymbol{e}_i(t)\|$

$-\beta_c\eta_i(t)\le\alpha_c\|\mathbb{X}_i(t)\|$. Therefore, $\frac{\rho_c}{\alpha_c}\|\boldsymbol{\Phi}_c\boldsymbol{e}_i(t)\|-\beta_c\frac{\rho_c}{\alpha_c}\eta_i(t)\le\rho_c\|\mathbb{X}_i(t)\|$. Incorporating this inequality in (7), results in $\dot\eta_i(t)\ge-\left(\gamma_c+\beta_c\frac{\rho_c}{\alpha_c}\right)\eta_i(t)+\frac{\rho_c}{\alpha_c}\|\boldsymbol{\Phi}_c\boldsymbol{e}_i(t)\|$. Hence, $\dot\eta_i(t)\ge-(\gamma_c+\beta_c\frac{\rho_c}{\alpha_c})\eta_i(t)$. Thus, $\eta_i(t)>\eta_i\left(t^i_{k^{[i]}}\right)e^{-\left(\gamma_c+\beta_c\frac{\rho_c}{\alpha_c}\right)\left(t-t^i_{k^{[i]}}\right)}$. By induction and moving back through all events $t^i_{k^{[i]}}$, $t^i_{k^{[i]}-1}$, …, $t^i_0=0$, one obtains $\eta_i(t)>\eta_i(0)e^{-\left(\gamma_c+\beta_c\frac{\rho_c}{\alpha_c}\right)t}$ referring to its positive value. ■

Next, we obtain the minimum inter-event time (MIET) for leaders which excludes the Zeno-behaviour. The MIET for followers can be obtained in a similar way.

Theorem 1: The minimum inter-event time for leader i, ($\forall i\in\mathcal{L}$), is strictly positive and lower-bounded by

$$t^i_{k^{[i]}+1}-t^i_{k^{[i]}}\ge\frac{1}{\|\boldsymbol{A}\|}\ln\left(1+\|\boldsymbol{A}\|(\kappa_{1i}+\kappa_{2i})\right),\quad(i\in\mathcal{L}) \tag{25}$$

where

$$\kappa_{1i}=\frac{\alpha_1}{\kappa_{3i}}\left\|\mathbb{X}_i\left(t^i_{k^{[i]}+1}\right)\right\|\quad\kappa_{2i}=\frac{\beta_1}{\kappa_{3i}}\eta_i(0)e^{-\left(\gamma_1+\beta_1\frac{\rho_1}{\alpha_1}\right)t^i_{k^{[i]}+1}}$$
$$\kappa_{3i}=\|\boldsymbol{\Phi}_1\|\left(\|\boldsymbol{B}\boldsymbol{K}_1\|\|\mathbb{X}_i\left(t^i_{k^{[i]}+1}\right)\|+\kappa_{4i}\right)$$
$$\kappa_{4i}=\left\|\boldsymbol{B}\boldsymbol{H}\sum_{j\in\mathcal{N}^i_{\mathcal{L}\leftarrow\mathcal{L}}}\mathfrak{a}_{i,j}(\boldsymbol{h}_i-\boldsymbol{h}_j)\right\|. \tag{26}$$

Proof: Consider $t^i_{k^{[i]}}$ and $t^i_{k^{[i]}+1}$ as two consecutive events for leader i. From (6), it holds that $\left\|\boldsymbol{e}_i\left(t^i_{k^{[i]}}\right)\right\|=0$. For $t\ge t^i_{k^{[i]}}$, the state error $\boldsymbol{e}_i(t)$ evolves from zero until the next event is triggered at $t=t^i_{k^{[i]}+1}$ which fulfills (6). From $\boldsymbol{e}_i(t)=\boldsymbol{\Lambda}_i(t)\hat{\boldsymbol{x}}_i(t)-\boldsymbol{x}_i(t)$, it follows that $\dot{\boldsymbol{e}}_i(t)=\boldsymbol{A}\boldsymbol{\Lambda}_i(t)\hat{\boldsymbol{x}}_i(t)-\dot{\boldsymbol{x}}_i(t)$. From (8) and (1), we obtain that $\dot{\boldsymbol{x}}_i(t)=\boldsymbol{A}\boldsymbol{x}_i(t)+\boldsymbol{B}\boldsymbol{K}_1\mathbb{X}_i(t)+\boldsymbol{B}\boldsymbol{H}\sum_{j\in\mathcal{N}^i_{\mathcal{L}\leftarrow\mathcal{L}}}\mathfrak{a}_{i,j}(\boldsymbol{h}_i-\boldsymbol{h}_j)$. After simplifying one gets $\dot{\boldsymbol{e}}_i(t)=\boldsymbol{A}\boldsymbol{e}_i(t)-\boldsymbol{B}\boldsymbol{K}_1\mathbb{X}_i(t)-\boldsymbol{B}\boldsymbol{H}\sum_{j\in\mathcal{N}^i_{\mathcal{L}\leftarrow\mathcal{L}}}\mathfrak{a}_{i,j}(\boldsymbol{h}_i-\boldsymbol{h}_j)$, or $\|\dot{\boldsymbol{e}}_i(t)\|\le\|\boldsymbol{A}\|\|\boldsymbol{e}_i(t)\|+\|\boldsymbol{B}\boldsymbol{K}_1\|\|\mathbb{X}_i(t)\|+\kappa_{4i}$, $t\in[t^i_{k^{[i]}},t^i_{k^{[i]}+1})$. It, then, follows that:

$$\|\boldsymbol{e}_i(t)\|\le\frac{\|\boldsymbol{B}\boldsymbol{K}_1\|\|\mathbb{X}_i(t)\|+\kappa_{4i}}{\|\boldsymbol{A}\|}\left(e^{\|\boldsymbol{A}\|\left(t-t^i_{k^{[i]}}\right)}-1\right). \tag{27}$$

The next event is triggered by (6) at $t=t^i_{k^{[i]}+1}$ where $\|\boldsymbol{\Phi}_1\boldsymbol{e}_i\left(t^i_{k^{[i]}+1}\right)\|=\alpha_1\|\mathbb{X}_i\left(t^i_{k^{[i]}+1}\right)\|+\beta_1\eta_i\left(t^i_{k^{[i]}+1}\right)$. Then, from Lemma 1, it follows that $\|\boldsymbol{e}_i\left(t^i_{k^{[i]}+1}\right)\|\ge\frac{\alpha_1}{\|\boldsymbol{\Phi}_1\|}\|\mathbb{X}_i\left(t^i_{k^{[i]}+1}\right)\|+\frac{\beta_1}{\|\boldsymbol{\Phi}_1\|}\eta_i(0)e^{-\left(\gamma_1+\beta_1\frac{\rho_1}{\alpha_1}\right)t^i_{k^{[i]}+1}}$. The latter inequality together with (27) leads to (25). The right hand side of (25) is strictly positive. Therefore, the minimum time between two events is strictly positive. Hence, DEM (6) does not exhibit the Zeno-behaviour. ■

Corollary 1: It is straightforward to show that the MIET for followers is obtained from (25) by considering $\kappa_{4i}=0$, ($i\in\mathcal{F}$), and replacing the followers' parameters $\boldsymbol{K}_2$, $\boldsymbol{\Phi}_2$, α_2, β_2, γ_2, and ρ_2.

One approach to reduce the frequency of events (Design objective 1 mentioned in Section II-C), is to increase the value of MIET (25). To this end, one should limit $\{\|\boldsymbol{K}_c\|,\|\boldsymbol{\Phi}_c\|,\gamma_c\}$ and increase $\{\alpha_c,\beta_c,\rho_c\}$ for $c\in\{1,2\}$. On the other hand, the formation-containment convergence rate (Design objective 2) is impacted by $\|\boldsymbol{K}_c\|$. Accelerating the convergence rate, for example, tends to increase $\|\boldsymbol{K}_c\|$, which decreases MIET (25). As mentioned previously, increasing the MIET tends to reduce $\|\boldsymbol{K}_c\|$, which may lead to a conservative convergence rate. To cope with the trade-off between the frequency of the events and convergence of the MAS, it is desirable to design unknown parameters using an optimization framework (Design objectives 3 and 4) based on an objective function that increases the inter-event interval for a desired convergence rate for formation-containment.

B. Parameter Optimization for Leaders

In this section, we propose an optimization to co-design all required parameters ($\boldsymbol{K}_1$, $\boldsymbol{\Phi}_1$, α_1, β_1, γ_1, and ρ_1) for the leaders. To solve the optimization, each leader should locally estimate the eigenvalues of $\boldsymbol{L}_{\mathcal{L}}$ (included in $\tilde{\boldsymbol{J}}_1$) and its matrix of eigenvectors $\boldsymbol{W}$ as a preliminary step. These eigenparameters can be estimated in a distributed fashion using [40].

Theorem 2: Let the formation gain $\boldsymbol{H}$ and formation vectors $\boldsymbol{h}_i$ satisfy the formability condition (15). Given (15) and a desired convergence rate ζ_1, if there exist matrices $\boldsymbol{P}\in\mathbb{R}^{n\times n}>0$, $\tilde{\boldsymbol{\Phi}}\in\mathbb{R}^{n\times n}>0$, $\boldsymbol{\Omega}\in\mathbb{R}^{m\times n}$, positive scalars $\tilde\alpha$, $\tilde\beta$, $\tilde\gamma$, $\tilde\rho$, τ_1, τ_2, and θ_c ($1\le c\le 7$), satisfying the following optimization:

$$\min\mathbb{F}_1=\sum_{c=1}^{7}\theta_c \tag{28}$$

s.t.

$$\boldsymbol{\Xi}=\begin{bmatrix}\boldsymbol{\Xi}_{11}&\widetilde{\boldsymbol{J}}_1\widetilde{\boldsymbol{W}}\otimes\boldsymbol{B}\boldsymbol{\Omega}&\widetilde{\boldsymbol{J}}_1\otimes\boldsymbol{P}&\boldsymbol{0}\\ *&-\boldsymbol{I}_M\otimes\tilde{\boldsymbol{\Phi}}&\boldsymbol{0}&\boldsymbol{I}_M\otimes\boldsymbol{P}\\ *&*&-\tau_1\boldsymbol{I}&\boldsymbol{0}\\ *&*&*&-\tau_2\boldsymbol{I}\end{bmatrix}<0$$
$$\pi_1=1-2\tilde\gamma+2\tilde\beta+2\zeta_1<0$$
$$\pi_2=4\tilde\alpha+2\tilde\rho+(-2+\tau_1)<0$$
$$\boldsymbol{\pi}_3=(4\tilde\alpha+2\tilde\rho)\widetilde{\boldsymbol{J}}_1^2+(-2+\tau_2)\boldsymbol{I}_{M-1}<0$$
$$\begin{bmatrix}\theta_1\boldsymbol{I}&\boldsymbol{I}\\ *&\boldsymbol{P}\end{bmatrix}>0\quad\begin{bmatrix}-\theta_2\boldsymbol{I}&\tilde{\boldsymbol{\Phi}}\\ *&-\boldsymbol{I}\end{bmatrix}<0\quad\begin{bmatrix}\theta_3&1\\ *&\tilde\alpha\end{bmatrix}>0$$
$$\begin{bmatrix}\theta_4&1\\ *&\tilde\beta\end{bmatrix}>0\quad\begin{bmatrix}-\theta_5&\tilde\gamma\\ *&-1\end{bmatrix}<0\quad\begin{bmatrix}\theta_6&1\\ *&\tilde\rho\end{bmatrix}>0$$
$$\begin{bmatrix}-\theta_7\boldsymbol{I}&\boldsymbol{\Omega}\\ *&-\boldsymbol{I}\end{bmatrix}<0 \tag{29}$$

where $\boldsymbol{\Xi}_{11}=\boldsymbol{I}_{M-1}\otimes(\boldsymbol{P}\boldsymbol{A}^T+\boldsymbol{A}\boldsymbol{P})+\tilde{\boldsymbol{J}}_1\otimes\boldsymbol{B}\boldsymbol{\Omega}+(\tilde{\boldsymbol{J}}_1\otimes\boldsymbol{B}\boldsymbol{\Omega})^T+2\zeta_1\boldsymbol{I}_{M-1}\otimes\boldsymbol{P}$, then design parameters for leaders are computed as

$$\begin{array}{lll}\boldsymbol{K}_1=\boldsymbol{\Omega}\boldsymbol{P}^{-1}&\boldsymbol{\Phi}_1=(\boldsymbol{P}^{-1}\tilde{\boldsymbol{\Phi}}\boldsymbol{P}^{-1})^{1/2}&\alpha_1=\sqrt{\tilde\alpha}\\ \beta_1=\sqrt{\tilde\beta}&\gamma_1=\tilde\gamma&\rho_1=\sqrt{\tilde\rho}.\end{array} \tag{30}$$

Using design parameters (30), system trajectories converge at a rate which satisfies the following inequality:

$$\lambda_{\min}(\boldsymbol{P}^{-1})\boldsymbol{\psi}^T_{\mathcal{L}}(t)\boldsymbol{\psi}_{\mathcal{L}}(t)+\boldsymbol{\eta}^T_{\mathcal{L}}(t)\boldsymbol{\eta}_{\mathcal{L}}(t)\le\mu e^{-2\zeta_1 t} \tag{31}$$

where $\mu=\lambda_{\max}(\boldsymbol{P}^{-1})\boldsymbol{\psi}^T_{\mathcal{L}}(0)\boldsymbol{\psi}_{\mathcal{L}}(0)+\boldsymbol{\eta}^T_{\mathcal{L}}(0)\boldsymbol{\eta}_{\mathcal{L}}(0)$. The following bounds are guaranteed by minimizing $\mathbb{F}_1$:

$$\|\boldsymbol{K}_1\| \le \theta_1 \sqrt{\theta_7} \quad \|\boldsymbol{\Phi}_1\| \le \theta_1 \theta_2^{1/4} \quad \alpha_1 \ge \frac{1}{\sqrt{\theta_3}} \quad \beta_1 \ge \frac{1}{\sqrt{\theta_4}}$$
$$\gamma_1 \le \sqrt{\theta_5} \qquad \rho_1 \ge \frac{1}{\sqrt{\theta_6}}. \tag{32}$$

Proof: The proof is included in Appendix A. ■

C. Parameter Optimization for Followers

In the following theorem, we co-design all required parameters ($\boldsymbol{K}_2$, $\boldsymbol{\Phi}_2$. α_2, β_2, γ_2, and ρ_2) for the followers. The following optimization is based on the knowledge of the eigenvalues and eigenvectors of $\boldsymbol{L}_{\mathcal{F}}$. The eigenvalues of $\boldsymbol{L}_{\mathcal{F}}$ are equal to non-zero eigenvalues of $\boldsymbol{L}_{\text{est}} = [\boldsymbol{L}_{\mathcal{F}} \;\; \boldsymbol{L}_{\mathcal{FL}}; \boldsymbol{0} \;\; \boldsymbol{0}]$. The eigenvalues of $\boldsymbol{L}_{\text{est}}$ can be computed by the followers in a distributed fashion using [40].

Theorem 3: Let the formability condition (15) hold. Given (15) and a desired convergence rate ζ_2, if there exist matrices $\boldsymbol{P} \in \mathbb{R}^{n\times n} > 0$, $\tilde{\boldsymbol{\Phi}} \in \mathbb{R}^{n\times n} > 0$, $\boldsymbol{\Omega} \in \mathbb{R}^{m\times n}$, positive scalars $\tilde{\alpha}$, $\tilde{\beta}$, $\tilde{\gamma}$, $\tilde{\rho}$, τ_1, τ_2, and θ_c, $(1 \le c \le 7)$, satisfying the following optimization[1]:

$$\min \mathbb{F}_2 = \sum_{c=1}^{7} \theta_c \tag{33}$$

s.t.

$$\boldsymbol{\Xi} = \begin{bmatrix} \boldsymbol{\Xi}_{11} & \boldsymbol{J}_2 \boldsymbol{V}^{-1} \otimes \boldsymbol{B}\boldsymbol{\Omega} & \boldsymbol{I}_N \otimes \boldsymbol{P} & \boldsymbol{0} \\ * & -\boldsymbol{I}_N \otimes \tilde{\boldsymbol{\Phi}} & \boldsymbol{0} & \boldsymbol{I}_N \otimes \boldsymbol{P} \\ * & * & -\tau_1 \boldsymbol{I} & \boldsymbol{0} \\ * & * & * & -\tau_2 \boldsymbol{I} \end{bmatrix} < 0$$
$$\pi_1 = 1 - 2\tilde{\gamma} + 2\tilde{\beta} + 2\zeta_2 < 0$$
$$\pi_2 = 4\tilde{\alpha} + 2\tilde{\rho} + (-2 + \tau_1) \quad < 0$$
$$\boldsymbol{\pi}_3 = (4\tilde{\alpha} + 2\tilde{\rho})\boldsymbol{J}_2^2 + (-2 + \tau_2)\boldsymbol{I}_N < 0$$
$$\begin{bmatrix} \theta_1 \boldsymbol{I} & \boldsymbol{I} \\ * & \boldsymbol{P} \end{bmatrix} > 0 \quad \begin{bmatrix} -\theta_2 \boldsymbol{I} & \tilde{\boldsymbol{\Phi}} \\ * & -\boldsymbol{I} \end{bmatrix} < 0 \quad \begin{bmatrix} \theta_3 & 1 \\ * & \tilde{\alpha} \end{bmatrix} > 0$$
$$\begin{bmatrix} \theta_4 & 1 \\ * & \tilde{\beta} \end{bmatrix} > 0 \quad \begin{bmatrix} -\theta_5 & \tilde{\gamma} \\ * & -1 \end{bmatrix} < 0 \quad \begin{bmatrix} \theta_6 & 1 \\ * & \tilde{\rho} \end{bmatrix} > 0$$
$$\begin{bmatrix} -\theta_7 \boldsymbol{I} & \boldsymbol{\Omega} \\ * & -\boldsymbol{I} \end{bmatrix} < 0 \tag{34}$$

where $\boldsymbol{\Xi}_{11} = \boldsymbol{I}_N \otimes (\boldsymbol{P}\boldsymbol{A}^T + \boldsymbol{A}\boldsymbol{P}) + \boldsymbol{J}_2 \otimes \boldsymbol{B}\boldsymbol{\Omega} + (\boldsymbol{J}_2 \otimes \boldsymbol{B}\boldsymbol{\Omega})^T + 2\zeta_2 \boldsymbol{I}_N \otimes \boldsymbol{P}$, then design parameters for followers are computed as:

$$\boldsymbol{K}_2 = \boldsymbol{\Omega}\boldsymbol{P}^{-1} \quad \boldsymbol{\Phi}_2 = (\boldsymbol{P}^{-1}\tilde{\boldsymbol{\Phi}}\boldsymbol{P}^{-1})^{1/2} \quad \alpha_2 = \sqrt{\tilde{\alpha}}$$
$$\beta_2 = \sqrt{\tilde{\beta}} \qquad \gamma_2 = \tilde{\gamma} \qquad \rho_2 = \sqrt{\tilde{\rho}}. \tag{35}$$

The following bounds are guaranteed by minimizing $\mathbb{F}_2$:

$$\|\boldsymbol{K}_2\| \le \theta_1 \sqrt{\theta_7} \quad \|\boldsymbol{\Phi}_2\| \le \theta_1 \theta_2^{1/4} \quad \alpha_2 \ge \frac{1}{\sqrt{\theta_3}} \quad \beta_2 \ge \frac{1}{\sqrt{\theta_4}}$$
$$\gamma_2 \le \sqrt{\theta_5} \qquad \rho_2 \ge \frac{1}{\sqrt{\theta_6}}. \tag{36}$$

Proof: The proof is included in Appendix B. ■

[1] To improve comprehension, common notation used for leaders and followers is intentionally kept the same in Theorems 2 and 3. For example, $\boldsymbol{\Xi}$ in Theorem 2 corresponds to the constraint matrix for the leaders. Likewise, $\boldsymbol{\Xi}$ in Theorem 3 corresponds to the constraint matrix for the followers. The difference between them is evident from the context where the symbols are used.

Based on Theorems 2 and 3, the proposed formation-containment control using dynamic event-triggered mechanism (FCC/DEME) is summarized in Algorithm 1.

Remark 6: We note that the parameter design stage in FCC/DEME is independent of $\boldsymbol{L}_{\mathcal{FL}}$. Therefore, the communication topology between the leaders and followers can change during the formation-containment process without requiring a re-design of the control and event-triggering parameters. In other words, the leader-to-follower transmission can be performed by different leaders at each period of time. This prolongs the leaders' communication energy resources since one subset of leaders can transmit to the followers for a certain time interval. Then, this subset ceases the leader-to-follower transmission and another subset takes the responsibility of transmitting to the followers.

Algorithm 1 FCC/DEME

I(a) Parameter Design (Leaders): D1–D3

D1. Formation gain $\boldsymbol{H}$ is selected such that the formability condition (15) is satisfied for formation vectors $\boldsymbol{h}_i$.

D2. Each leader uses a distributed approach such as [40], [41] to locally estimate eigenvalues and eigenvectors of $\boldsymbol{L}_{\mathcal{L}}$. Then, they construct $\tilde{\boldsymbol{J}}_1$ and $\tilde{\boldsymbol{W}}$ following Section III-B.

D3. Each leader solves optimization (28) for an agreed value of ζ_1. The control gain and dynamic event-triggering parameters are computed from (30).

I(b) Parameter Design (Followers): D1 and D2

D1. Each follower uses a distributed approach [40], [41] to locally estimate eigenvalues and eigenvectors of $\boldsymbol{L}_{\mathcal{F}}$.

D2. Followers solve optimization (33) for an agreed value of ζ_2. The control gain and event-triggering parameters are computed from (35).

II Execution: E1 and E2

E1. Leaders and followers transmit their initial state values $\boldsymbol{x}_i(0)$ to their neighbourhoods.

E2. Using designed parameters the states of the leaders approach the desired formation specified by formation vectors $\boldsymbol{h}_i$. The followers achieve the event-triggered containment.

V. Simulations

In this section, we conduct simulations to evaluate the performance of the proposed formation-containment implementation. The YALMIP parser and SDPT3 solver are used to solve the proposed optimizations.

1) Multi-Agent System Dynamics: We test FCC/DEME for a MAS comprising of 4 leader and 6 follower robots as shown in Fig. 3. The dynamics of each robot [42] is

$$\dot{\bar{\boldsymbol{x}}}_i = \boldsymbol{f}(\bar{\boldsymbol{x}}_i) + \bar{\boldsymbol{B}}\bar{\boldsymbol{u}}_i, \quad (1 \le i \le 10) \tag{37}$$

where

$$\bar{\boldsymbol{x}}_i = \left[r_{x,i}, r_{y,i}, \theta_i, v_i, \omega_i\right]^T$$
$$\boldsymbol{f}(\bar{\boldsymbol{x}}_i) = [v_i \cos(\theta_i), v_i \sin(\theta_i), \omega_i, 0, 0]^T$$
$$\bar{\boldsymbol{B}} = \begin{bmatrix} 0 & 0 & 0 & 0 & \frac{1}{J} \\ 0 & 0 & 0 & \frac{1}{m} & 0 \end{bmatrix}^T, \qquad \bar{\boldsymbol{u}}_i = [f_i, \tau_i]^T.$$

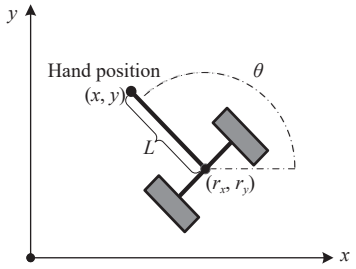

Fig. 3. Non-holonomic mobile robot coordinates.

For robot i, parameters $r_{x,i}$ and $r_{y,i}$ are the inertial positions; θ_i is the orientation; v_i is the linear speed; ω_i is the angular speed; τ_i is the applied torque; f_i is the applied force; $m=$ 10.1 kg is the mass; and $J=0.13$ kg $\bullet$m^2 is the moment of inertia [42].

We use the network topology shown in Fig. 1 which is represented by the partitioned Laplacian matrices (3). It holds that

$$\widetilde{\boldsymbol{J}}_1=\text{diag}(2,2,4)$$

$$\boldsymbol{J}_2=\text{diag}(4.613,3.808,3.258,0.387,1.192,1.742)$$

$$\widetilde{\boldsymbol{W}}=\begin{bmatrix}0.707 & 0 & -0.707 & 0\\ 0 & 0.707 & 0 & -0.707\\ -0.5 & 0.5 & -0.5 & 0.5\end{bmatrix}$$

$$\boldsymbol{V}^{-1}=\begin{bmatrix}0.354 & 0.261 & -0.300 & -0.381 & 0.524 & -0.544\\ 0.216 & 0.355 & 0.064 & -0.707 & -0.472 & 0.317\\ 0.425 & -0.413 & 0.565 & -0.046 & -0.299 & -0.488\\ -0.381 & -0.544 & -0.524 & -0.354 & -0.300 & -0.261\\ 0.707 & -0.317 & -0.472 & 0.216 & -0.064 & 0.355\\ -0.046 & -0.488 & 0.299 & -0.425 & 0.565 & 0.413\end{bmatrix}.$$

The formation-containment objective in this example is that the 4 leaders in (37) form a regular square and the 6 followers merge within the square form by the leaders.

2) Feedback Linearization: As shown in [42], robot (37) is state feedback linearizable. To this end, denote the following variables:

$$\begin{aligned}&x_{1,i}=r_{x,i}+L\cos(\theta_i) && x_{2,i}=r_{y,i}+L\sin(\theta_i)\\ &x_{3,i}=v_i\cos(\theta_i)-L\omega_i\sin(\theta_i) && x_{4,i}=v_i\sin(\theta_i)+L\omega_i\cos(\theta_i)\\ &x_{5,i}=\theta_i\end{aligned} \tag{38}$$

where $L=0.12$ m is an internal distance in the structure of the robot as shown in Fig. 3. Now, consider the following linear system:

$$\dot{\boldsymbol{x}}_i=\boldsymbol{A}\boldsymbol{x}_i+\boldsymbol{B}\boldsymbol{u}_i \quad (1\le i\le 10), \tag{39}$$

where $\boldsymbol{x}_i=[\,x_{1,i},\,x_{2,i},\,x_{3,i},\,x_{4,i}\,]^T$ and

$$\boldsymbol{A}=\begin{bmatrix}0&0&1&0\\0&0&0&1\\0&0&0&0\\0&0&0&0\end{bmatrix} \qquad \boldsymbol{B}=\begin{bmatrix}0&0\\0&0\\1&0\\0&1\end{bmatrix}. \tag{40}$$

The feedback linearizing control for robot i is

$$\bar{\boldsymbol{u}}_i=\begin{bmatrix}\frac{1}{m}\cos(\theta_i) & -\frac{L}{J}\sin(\theta_i)\\ \frac{1}{m}\sin(\theta_i) & \frac{L}{J}\cos(\theta_i)\end{bmatrix}^{-1} \times\left(\boldsymbol{u}_i-\begin{bmatrix}-v_i\omega_i\sin(\theta_i)-L\omega_i^2\cos(\theta_i)\\ v_i\omega_i\cos(\theta_i)-L\omega_i^2\sin(\theta_i)\end{bmatrix}\right). \tag{41}$$

Following [42], the states of actual system (37) is obtained from the states of linear system (39) as:

$$\begin{aligned}&r_{x,i}=x_{1,i}-L\cos(x_{5,i}) && r_{y,i}=x_{2,i}-L\sin(x_{5,i})\\ &\theta_i=x_{5,i} && v_i=\frac{1}{2}x_{3,i}\cos(x_{5,i})+\frac{1}{2}x_{4,i}\sin(x_{5,i})\\ &\omega_i=-\frac{1}{2L}x_{3,i}\sin(x_{5,i})+\frac{1}{2L}x_{4,i}\cos(x_{5,i})\end{aligned} \tag{42}$$

where $\dot{x}_{5,i}=-\frac{1}{2L}x_{3,i}\sin(x_{5,i})+\frac{1}{2L}x_{4,i}\cos(x_{5,i})$. To solve formation-containment for the nonlinear MAS (37), one can design a control protocol for linear system (39) with control input $\boldsymbol{u}_i$. Trajectories of system (37), then, follows (42) if the feedback linearizing control (41) is applied.

3) Formation Vector and Formation Gain: As specified previously, the 4 leaders in (37) are supposed to form a regular square. According to Definition 1, when formation is achieved it holds that

$$\lim_{t\to\infty}(\boldsymbol{x}_i-\boldsymbol{x}_{i+1})=\boldsymbol{h}_i-\boldsymbol{h}_{i+1}, \quad (1\le i\le M-1). \tag{43}$$

To compute formation vectors $\boldsymbol{h}_i$, we remind that the M vertices of a 2-dimensional M-sided regular polygon with edge d, centered at $(0,0)$, can be given by $p_i=(p_{i,x},p_{i,y})$, where $p_{i,x}=d\cos(2\pi i/M)$ and $p_{i,y}=d\sin(2\pi i/M)$ for $(1\le i\le M)$. We assume that the position states of leader i (i.e., $x_{1,i}$ and $x_{2,i}$) converge to vertice i of the square. Additionally, the velocity states of all leader converge to constant values (i.e., $x_{3,i}=x_{3,j}=\bar{x}_3$ and $x_{4,i}=x_{4,j}=\bar{x}_4$, $1\le i,j\le M$). Therefore, the steady-state for leader i converges to the following vector:

$$\lim_{t\to\infty}\boldsymbol{x}_i=\left[p_{x,i},p_{y,i},\bar{x}_3,\bar{x}_4\right]^T. \tag{44}$$

The following equality holds from (43) in the steady state:

$$\left[p_{x,i},p_{y,i},\bar{x}_3,\bar{x}_4\right]^T-\left[p_{x,i+1},p_{y,i+1},\bar{x}_3,\bar{x}_4\right]^T=\boldsymbol{h}_i-\boldsymbol{h}_{i+1} \tag{45}$$

for $(1\le i\le M-1)$. Based on (45) and considering $\boldsymbol{h}_1=[0,0,0,0]^T$, the remaining formation vectors are computed iteratively as follows:

$$\boldsymbol{h}_{i+1}=\boldsymbol{h}_i-\boldsymbol{b}_i, \quad (1\le i\le M-1) \tag{46}$$

where $\boldsymbol{b}_i$ is the left-hand side of (45) and equals

$$\boldsymbol{b}_i=d\left[\cos\frac{2\pi i}{M}-\cos\frac{2\pi(i+1)}{M},\sin\frac{2\pi i}{M}-\sin\frac{2\pi(i+1)}{M},0,0\right]^T.$$

with $M=4$ and $d=3$, the leaders in this example will form a regular square with an edge of $d=3$ m. From (40) and (46), it is straightforward to show that $\boldsymbol{A}\sum_{j\in\mathcal{N}_{\mathcal{L}\leftarrow\mathcal{L}}^i}(\boldsymbol{h}_i-\boldsymbol{h}_j)=\boldsymbol{0}$, $(1\le i\le 4)$, which implies that the formability condition (15) holds with $\boldsymbol{H}=\boldsymbol{0}$. Therefore, the formation gain in (8) is considered as $\boldsymbol{H}=\boldsymbol{0}$.

4) Parameter Design for Leaders: Let $\zeta_1 = 0.3$. Using the SDPT3 solver, optimization (28) is solved which leads to the following solution:

$$\boldsymbol{P} = \begin{bmatrix} 0.0675 & -0.0505 \\ * & 0.2057 \end{bmatrix} \otimes \boldsymbol{I}_2 \quad \widetilde{\boldsymbol{\Phi}} = \begin{bmatrix} 1.1849 & -0.0437 \\ * & 1.4451 \end{bmatrix} \otimes \boldsymbol{I}_2$$

$$\boldsymbol{\Omega} = \begin{bmatrix} -0.0144 & -0.1971 \end{bmatrix} \otimes \boldsymbol{I}_2 \quad \tilde{\alpha} = 0.0178$$

$$\tilde{\beta} = 0.5980 \quad \tilde{\gamma} = 1.3980 \quad \tilde{\rho} = 0.0252 \quad \tau_1 = 1.8783$$

$$\tau_2 = 0.0536 \quad \theta_1 = 19.6111 \quad \theta_2 = 2.1089 \quad \theta_3 = 56.1314$$

$$\theta_4 = 1.6721 \quad \theta_5 = 1.9545 \quad \theta_6 = 39.6909 \quad \theta_7 = 0.0391.$$

Design parameters are calculated form (30) as follows:

$$\boldsymbol{K}_1 = -[1.1414, 1.2390] \otimes \boldsymbol{I}_2 \quad \boldsymbol{\Phi}_1 = \begin{bmatrix} 19.7233 & 4.8133 \\ * & 7.0278 \end{bmatrix} \otimes \boldsymbol{I}_2$$

$$\alpha_1 = 0.1335 \quad \beta_1 = 0.7733 \quad \gamma_1 = 1.3980 \quad \rho_1 = 0.1587.$$

The value of the objective function is $\mathbb{F}_1 = 121.20$.

5) Parameter Design for Followers: Next, we compute design parameters for the followers. We solve optimization (33) with $\zeta_2 = 0.3$ which leads to the following solution:

$$\boldsymbol{P} = \begin{bmatrix} 0.1844 & -0.0837 \\ * & 0.1605 \end{bmatrix} \otimes \boldsymbol{I}_2 \quad \tilde{\boldsymbol{\Phi}} = \begin{bmatrix} 1.6485 & -0.0651 \\ * & 1.7888 \end{bmatrix} \otimes \boldsymbol{I}_2$$

$$\boldsymbol{\Omega} = \begin{bmatrix} -0.0449 & -0.3973 \end{bmatrix} \otimes \boldsymbol{I}_2 \quad \tilde{\alpha} = 0.0134$$

$$\tilde{\beta} = 0.5980 \quad \tilde{\gamma} = 1.3980 \quad \tilde{\rho} = 0.0184 \quad \tau_1 = 1.9086$$

$$\tau_2 = 0.0544 \quad \theta_1 = 11.3746 \quad \theta_2 = 3.2921 \quad \theta_3 = 74.6831$$

$$\theta_4 = 1.6721 \quad \theta_5 = 1.9545 \quad \theta_6 = 52.8089 \quad \theta_7 = 0.1598.$$

The following design parameters are then computed:

$$\boldsymbol{K}_2 = -[1.7906, 3.4091] \otimes \boldsymbol{I}_2 \quad \boldsymbol{\Phi}_2 = \begin{bmatrix} 9.0799 & 4.6743 \\ * & 10.7708 \end{bmatrix} \otimes \boldsymbol{I}_2$$

$$\alpha_2 = 0.1157 \quad \beta_2 = 0.7733 \quad \gamma_2 = 1.3980 \quad \rho_2 = 0.1376.$$

The objective function is computed as $\mathbb{F}_2 = 145.94$.

6) Formation-Containment Implementation: Let $\boldsymbol{x}_1(0) = [-10, -4, 0, 0]^T$, $\boldsymbol{x}_2(0) = [-6, -4, 0, 0]^T$, $\boldsymbol{x}_3(0) = [3, -8, 0, 0]^T$, $\boldsymbol{x}_4(0) = [10, -2, 0, 0]^T$, $\boldsymbol{x}_5(0) = [-5, 8, 0, 0]^T$, $\boldsymbol{x}_6(0) = [5, 8, 0, 0]^T$, $\boldsymbol{x}_7(0) = [0, 0, 0, 0]^T$, $\boldsymbol{x}_8(0) = [3, 0, 0, 0]^T$, $\boldsymbol{x}_9(0) = [1.5, 2, 0, 0]^T$, $\boldsymbol{x}_{10}(0) = [3, 3, 0, 0]^T$, and $\eta_i(0) = 1$, $(1 \le i \le 10)$. We use the following criterion to determine $t^\star$ which is the time when formation-containment is achieved. Time $t^\star$ is determined as follows:

$$t^\star = \inf\{\ t\ \mid \max\left\{\frac{\|\boldsymbol{\psi}_{\mathcal{L}}(t)\|}{\|\boldsymbol{\psi}_{\mathcal{L}}(0)\|}, \frac{\|\boldsymbol{\psi}_{\mathcal{F}}(t)\|}{\|\boldsymbol{\psi}_{\mathcal{F}}(0)\|}\right\} \le \delta\ \}. \qquad (47)$$

Conceptually speaking, time $t^\star$ is the smallest time when both the formation for leaders and containment for followers are achieved within at least δ factor of the initial disagreements specified by $\|\boldsymbol{\psi}_{\mathcal{L}}(0)\|$ and $\|\boldsymbol{\psi}_{\mathcal{F}}(0)\|$, respectively. This time, i.e., $t^\star$, is used as an index to compare the convergence rates for different examples. A larger value for $t^\star$ corresponds to a smaller rate of convergence and vice versa. We set $\delta = 0.005$ to provide a high accuracy for formation-containment achievement. For this setting, $t^\star = 12.72$ s with $\delta = 0.005$[2]. In Fig. 4, the trajectory of (37) is plotted where the leaders (shown in blue color) reach a regular square and the followers (shown in red color) achieve containment inside the square. The leaders, respectively, trigger 89, 75 104, and 69 events shown in Fig. 5(a). The number of events for the followers are, respectively, 69, 76, 79, 73, 83, and 80. The event instants for followers are shown in Fig. 5(b). The total average number of events (including both the leaders and followers) per agent is AE =79.70. We report the average inter-event time (AIET) computed by AIET = $t^\star$/AE. In this example, AIET = 0.1596. In fact, AIET measures the frequency of events. The minimum inter-event time (MIET) considering both the leaders and followers is MIET = 0.007 s in this example. As expected from Theorem 1, the MIET is strictly positive which rules out the possibility of the Zeno-behaviour. The trajectories of $\eta_i(t)$ $(1 \le i \le 10)$, are included in Figs. 6(a) and 6(b). As shown in Figs. 6(a) and 6(b), parameter $\eta_i(t)$ $(1 \le i \le 10)$, provides a considerable threshold for (6) and efficiently contributes in reducing the number of events. Variable $\eta_i(t)$ converges zero and does not cause steady-state error for formation-containment.

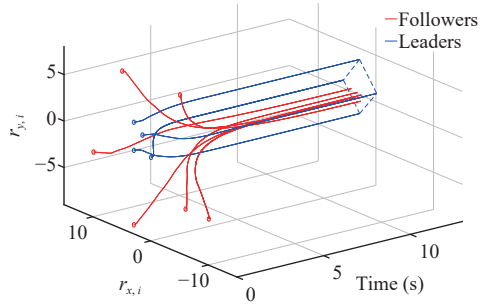

Fig. 4. Formation-containment for MAS (37).

7) Impact of Convergence Rates ζ_1 and ζ_2: In this section, we study the impact of different values for ζ_1 and ζ_2 on the formation-containment features. We solve (28) and (33) for the given values of ζ_1 and ζ_2 listed in Table I. Then, formation-containment for (37) is run using the designed parameters. According to Table I, we observe that:

i) With higher values for ζ_1 (or ζ_2) the rate of convergence increases and $t^\star$ steadily gets reduced. In return, the value AIET is also reduced which is translated to more dense event-triggerings.

ii) Larger values for ζ_1 (or ζ_2) lead to larger $\|\boldsymbol{K}_1\|$ (or $\|\boldsymbol{K}_2\|$). This is consistent with the fact that increasing the desired convergence rate requires higher values for the control input $\boldsymbol{u}_i(t)$.

iii) Larger values for ζ_1 (or ζ_2) lead to smaller values for $\{\alpha_1, \beta_1, \rho_1\}$ (or $\{\alpha_2, \beta_2, \rho_2\}$) and higher values for $\{\|\boldsymbol{\Phi}_1\|, \gamma_1\}$ (or $\{\|\boldsymbol{\Phi}_2\|, \gamma_2\}$) which together increase the frequency of the event-triggerings to cope with the higher given rate of convergence. The AIET, in return, becomes smaller (i.e.,

[2] It should be noted that convergence within 1% of the initial disagreement (i.e., $\delta = 0.01$ in (47)) provides a satisfactory level of formation-containment convergence in MAS (37). With $\delta = 0.01$, formation-containment is achieved at $t^\star = 9.43$ in this example. We run simulations using a higher accuracy of $\delta = 0.005$ to better observe the differences between different examples.

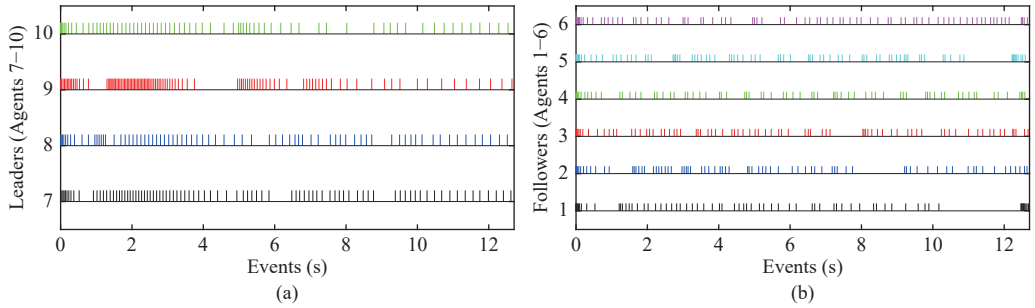

Fig. 5. Event instants (a) for leaders; (b) for followers.

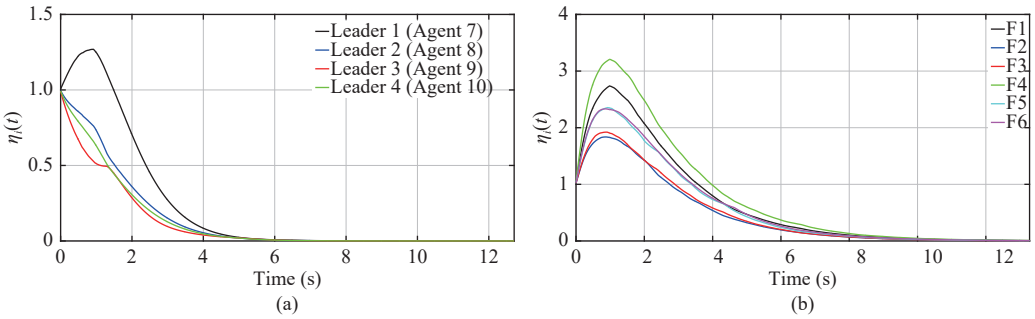

Fig. 6. Trajectory of the dynamic threshold $\eta_i(t)$, (a) for leaders; (b) for followers.

TABLE I
IMPACT OF DIFFERENT DESIRED CONVERGENCE RATES $\{\zeta_1,\zeta_2\}$ ON COMPUTED PARAMETERS AND FCC FEATURES.

Given rates		Computed parameters from Opt. (28)						Computed parameters from Opt. (33)						Features		
ζ_1	ζ_2	$\|\|\boldsymbol{K}_1\|\|$	$\|\|\boldsymbol{\Phi}_1\|\|$	α_1	β_1	γ_1	ρ_1	$\|\|\boldsymbol{K}_2\|\|$	$\|\|\boldsymbol{\Phi}_2\|\|$	α_2	β_2	γ_2	ρ_2	$t^\star$	AE	AIET
0.00	0.00	0.8904	13.36	0.1339	0.8107	1.1573	0.1592	2.4696	9.66	0.1161	0.8107	1.1573	0.1381	19.76	86.3	0.2290
0.10	0.10	1.1307	15.59	0.1338	0.7975	1.2360	0.1591	2.9551	11.14	0.1160	0.7975	1.2360	0.1379	17.17	80.2	0.2141
0.20	0.20	1.3949	18.22	0.1336	0.7851	1.3163	0.1589	3.4106	12.81	0.1159	0.7851	1.3163	0.1378	14.93	74.5	0.2004
0.30	0.30	1.6846	21.28	0.1335	0.7733	1.3980	0.1587	3.8507	14.67	0.1157	0.7733	1.3980	0.1376	12.72	79.7	0.1596
0.40	0.40	2.0011	24.78	0.1333	0.7623	1.4811	0.1585	4.2849	16.75	0.1156	0.7623	1.4810	0.1374	11.81	88.5	0.1334
0.50	0.50	2.3465	28.75	0.1331	0.7518	1.5652	0.1583	4.7201	19.04	0.1154	0.7518	1.5652	0.1372	10.44	95.6	0.1092

higher frequency for event-triggerings) as ζ_1 (or ζ_2) is increased.

These results verify the flexibility of FCC/DEME for formation-containment based on a structured trade-off between the rate of convergence and events frequency. We tested FCC/DEME for a variety of other multi-agent systems. The results corroborate the observations reported in the aforementioned simulation.

VI. CONCLUSION

Referred to as the FCC/DEME, this article proposes a formation-containment control implementation using the dynamic event-triggered strategy for multi-agent systems. To achieve formation for the leaders and containment for the followers, we transform the formation and containment formulations into stability problems of equivalent systems. The Lyapunov stability theorem is used to develop sufficient conditions to guarantee formation-containment. A novel objective function is proposed for optimal parameters design. Namely, the control gains and dynamic event-triggering parameters, are computed through a constrained convex optimization framework. Furthermore, it is verified that the dynamic event-triggering mechanism does not exhibit the Zeno-behavior. Finally, the effectiveness of FCC/DEME is studied through simulations for non-holonomic mobile robot multi-agent systems. Future work will extend the dynamic event-triggered mechanism to communication from the leaders to the followers.

APPENDIX A
PROOF OF THEOREM 2

To improve readability, we remove the time argument t in the proof. We note that all global vectors used in the proof are defined in (9).

Proof: Consider the following inequality:

$$\dot{V} + 2\zeta_1 V < 0 \tag{48}$$

where $V = V_1 + V_2$ with

$$V_1 = \boldsymbol{\psi}_{\mathcal{L}}^T \left(\boldsymbol{I}_{M-1} \otimes \boldsymbol{P}^{-1}\right) \boldsymbol{\psi}_{\mathcal{L}} \quad V_2 = \boldsymbol{\eta}_{\mathcal{L}}^T \boldsymbol{\eta}_{\mathcal{L}}. \tag{49}$$

Inequality (48) leads to the exponential convergence rate specified in (31). We obtain the time derivative for V_1

$$\dot{V}_1 = \boldsymbol{\psi}_{\mathcal{L}}^T \bar{\boldsymbol{\Xi}}_{11} \boldsymbol{\psi}_{\mathcal{L}} + 2\boldsymbol{\psi}_{\mathcal{L}}^T \bar{\boldsymbol{\Xi}}_{12} \boldsymbol{e}_{\mathcal{L}} \tag{50}$$

where

$$\bar{\boldsymbol{\Xi}}_{11} = \boldsymbol{I}_{M-1} \otimes (\boldsymbol{A}^T \boldsymbol{P}^{-1} + \boldsymbol{P}^{-1}\boldsymbol{A}) + 2\tilde{\boldsymbol{J}}_1 \otimes \boldsymbol{P}^{-1}\boldsymbol{B}\boldsymbol{K}_1$$
$$\bar{\boldsymbol{\Xi}}_{12} = \tilde{\boldsymbol{J}}_1 \tilde{\boldsymbol{W}} \otimes \boldsymbol{P}^{-1}\boldsymbol{B}\boldsymbol{K}_1.$$

In what follows $\dot{V}_2$ is expanded based on (7):

$$\dot{V}_2 = 2\boldsymbol{\eta}_{\mathcal{L}}^T(-\gamma_1 \boldsymbol{\eta}_{\mathcal{L}} + \rho_1 \bar{\mathbb{X}}_{\mathcal{L}}). \tag{51}$$

From Young's inequality, it holds that $\boldsymbol{\eta}_{\mathcal{L}}^T\left(\rho_1 \bar{\mathbb{X}}_{\mathcal{L}}\right) + \rho_1 \bar{\mathbb{X}}_{\mathcal{L}}^T \boldsymbol{\eta}_{\mathcal{L}} \le \boldsymbol{\eta}_{\mathcal{L}}^T \boldsymbol{\eta}_{\mathcal{L}} + \rho_1^2 \bar{\mathbb{X}}_{\mathcal{L}}^T \bar{\mathbb{X}}_{\mathcal{L}}$. We obtain the following upper-bound for (51):

$$\dot{V}_2 \le (1 - 2\gamma_1)\, \boldsymbol{\eta}_{\mathcal{L}}^T \boldsymbol{\eta}_{\mathcal{L}} + \rho_1^2 \bar{\mathbb{X}}_{\mathcal{L}}^T \bar{\mathbb{X}}_{\mathcal{L}}. \tag{52}$$

The global form of (4) for leaders can be viewed as follows:

$$\mathbb{X}_{\mathcal{L}} = \boldsymbol{L}_{\mathcal{L}} \otimes \boldsymbol{I}_n (\boldsymbol{\Lambda}_{\mathcal{L}} \hat{x}_{\mathcal{L}} - \boldsymbol{h}). \tag{53}$$

Knowing that $\boldsymbol{e}_{\mathcal{L}} = \boldsymbol{\Lambda}_{\mathcal{L}} \hat{x}_{\mathcal{L}} - \boldsymbol{x}_{\mathcal{L}}$, $\boldsymbol{z} = \boldsymbol{x}_{\mathcal{L}} - \boldsymbol{h}$, and $\boldsymbol{L}_{\mathcal{L}} = \tilde{\boldsymbol{W}}^{\dagger} \tilde{\boldsymbol{J}}_1 \tilde{\boldsymbol{W}}$, we develop the following expression from (13) and (53):

$$\mathbb{X}_{\mathcal{L}} = \left(\tilde{\boldsymbol{W}}^{\dagger} \tilde{\boldsymbol{J}}_1\right) \otimes \boldsymbol{I}_n \boldsymbol{\psi}_{\mathcal{L}} + \left(\tilde{\boldsymbol{W}}^{\dagger} \tilde{\boldsymbol{J}}_1 \tilde{\boldsymbol{W}}\right) \otimes \boldsymbol{I}_n \boldsymbol{e}_{\mathcal{L}}. \tag{54}$$

Considering that $\tilde{\boldsymbol{W}}^{\dagger T} \tilde{\boldsymbol{W}}^{\dagger} = \boldsymbol{I}$, we expand $\bar{\mathbb{X}}_{\mathcal{L}}^T \bar{\mathbb{X}}_{\mathcal{L}}$

$$\bar{\mathbb{X}}_{\mathcal{L}}^T \bar{\mathbb{X}}_{\mathcal{L}} = \mathbb{X}_{\mathcal{L}}^T \mathbb{X}_{\mathcal{L}} \le 2\boldsymbol{\sigma}_1^T \boldsymbol{\sigma}_1 + 2\boldsymbol{\sigma}_2^T \left(\tilde{\boldsymbol{J}}_1^2 \otimes \boldsymbol{I}_n\right) \boldsymbol{\sigma}_2 \tag{55}$$

where $\boldsymbol{\sigma}_1 = \left(\tilde{\boldsymbol{W}}^{\dagger} \tilde{\boldsymbol{J}}_1\right) \otimes \boldsymbol{I}_n \boldsymbol{\psi}_{\mathcal{L}}$ and $\boldsymbol{\sigma}_2 = \tilde{\boldsymbol{W}} \otimes \boldsymbol{I}_n \boldsymbol{e}_{\mathcal{L}}$. The following upper-bound holds from (52) and (55):

$$\dot{V}_2 \le (1-2\gamma_1)\boldsymbol{\eta}_{\mathcal{L}}^T \boldsymbol{\eta}_{\mathcal{L}} + 2\rho_1^2 \boldsymbol{\sigma}_1^T \boldsymbol{\sigma}_1 + 2\rho_1^2 \boldsymbol{\sigma}_2^T \left(\tilde{\boldsymbol{J}}_1^2 \otimes \boldsymbol{I}_n\right) \boldsymbol{\sigma}_2. \tag{56}$$

The following two equalities hold by definition:

$$\tau_1^{-1}\left(\boldsymbol{\psi}_{\mathcal{L}}^T \left(\tilde{\boldsymbol{J}}_1^2 \otimes \boldsymbol{I}_n\right) \boldsymbol{\psi}_{\mathcal{L}} - \boldsymbol{\sigma}_1^T \boldsymbol{\sigma}_1\right) = 0 \tag{57}$$

$$\tau_2^{-1}\left(\boldsymbol{e}_{\mathcal{L}}^T \boldsymbol{e}_{\mathcal{L}} - \boldsymbol{\sigma}_2^T \boldsymbol{\sigma}_2\right) \ge 0 \tag{58}$$

where $\tau_1 > 0$ and $\tau_2 > 0$ are decision variables. Based on (6), it holds that $\|\boldsymbol{\Phi}_1 \boldsymbol{e}_i(t)\| \le \alpha_1 \|\mathbb{X}_i(t)\| + \beta_1 \eta_i(t)$. Let $\boldsymbol{a}_1 = [\,\|\boldsymbol{\Phi}_1 \boldsymbol{e}_{N+1}(t)\|, \ldots, \|\boldsymbol{\Phi}_1 \boldsymbol{e}_{N+M}(t)\|\,]^T$. In a collective fashion it holds that $\boldsymbol{a}_1 \le \alpha_1 \bar{\mathbb{X}}_{\mathcal{L}} + \beta_1 \boldsymbol{\eta}_{\mathcal{L}}$, which is equivalent to

$$\begin{aligned} \boldsymbol{a}_1^T \boldsymbol{a}_1 = \boldsymbol{e}_{\mathcal{L}}^T \left(\boldsymbol{I}_M \otimes \boldsymbol{\Phi}_1^2\right) \boldsymbol{e}_{\mathcal{L}} &\le \left(\alpha_1 \bar{\mathbb{X}}_{\mathcal{L}} + \beta_1 \boldsymbol{\eta}_{\mathcal{L}}\right)^T \left(\alpha_1 \bar{\mathbb{X}}_{\mathcal{L}} + \beta_1 \boldsymbol{\eta}_{\mathcal{L}}\right) \\ &\le 2\alpha_1^2 \bar{\mathbb{X}}_{\mathcal{L}}^T \bar{\mathbb{X}}_{\mathcal{L}} + 2\beta_1^2 \boldsymbol{\eta}_{\mathcal{L}}^T \boldsymbol{\eta}_{\mathcal{L}}. \end{aligned} \tag{59}$$

Using (55), the following expression holds from (59):

$$\begin{aligned} \boldsymbol{e}_{\mathcal{L}}^T \left(\boldsymbol{I}_M \otimes \boldsymbol{\Phi}_1^2\right) \boldsymbol{e}_{\mathcal{L}} \le{}& 4\alpha_1^2 \boldsymbol{\sigma}_1^T \boldsymbol{\sigma}_1 + 4\alpha_1^2 \boldsymbol{\sigma}_2^T \left(\tilde{\boldsymbol{J}}_1^2 \otimes \boldsymbol{I}_n\right) \boldsymbol{\sigma}_2 \\ &+ 2\beta_1^2 \boldsymbol{\eta}_{\mathcal{L}}^T \boldsymbol{\eta}_{\mathcal{L}}. \end{aligned} \tag{60}$$

Let $\boldsymbol{\nu} = \left[\boldsymbol{\psi}_{\mathcal{L}}^T, \boldsymbol{e}_{\mathcal{L}}^T, \boldsymbol{\eta}_{\mathcal{L}}^T, \boldsymbol{\sigma}_1^T, \boldsymbol{\sigma}_2^T\right]^T$. Based on (50), (56)–(58), and (60), we re-arrange (48) as follows:

$$\boldsymbol{\nu}^T \begin{bmatrix} \tilde{\boldsymbol{\Xi}} & \boldsymbol{0} \\ * & \tilde{\boldsymbol{\Pi}} \end{bmatrix} \boldsymbol{\nu} < 0 \tag{61}$$

where $\tilde{\boldsymbol{\Xi}} = \begin{bmatrix} \tilde{\boldsymbol{\Xi}}_{11} & \bar{\boldsymbol{\Xi}}_{12} \\ * & \tilde{\boldsymbol{\Xi}}_{22} \end{bmatrix}$ and $\tilde{\boldsymbol{\Pi}} = \mathrm{diag}(\tilde{\boldsymbol{\pi}}_1, \tilde{\boldsymbol{\pi}}_2, \tilde{\boldsymbol{\pi}}_3)$ and

$$\begin{aligned} \tilde{\boldsymbol{\Xi}}_{11} &= \bar{\boldsymbol{\Xi}}_{11} + \tau_1^{-1} \tilde{\boldsymbol{J}}_1^2 \otimes \boldsymbol{I}_n + 2\zeta_1 \boldsymbol{I}_{M-1} \otimes \boldsymbol{P}^{-1} \\ \tilde{\boldsymbol{\Xi}}_{22} &= -\boldsymbol{I}_M \otimes \boldsymbol{\Phi}_1^2 + \tau_2^{-1} \boldsymbol{I}_{Mn} \\ \tilde{\boldsymbol{\pi}}_1 &= \left(1 - 2\gamma_1 + 2\beta_1^2 + 2\zeta_1\right) \boldsymbol{I}_M \\ \tilde{\boldsymbol{\pi}}_2 &= \left(2\rho_1^2 - \tau_1^{-1} + 4\alpha_1^2\right) \boldsymbol{I}_{Mn} \\ \tilde{\boldsymbol{\pi}}_3 &= -\tau_2^{-1} \boldsymbol{I} + \left(4\alpha_1^2 + 2\rho_1^2\right)\left(\tilde{\boldsymbol{J}}_1^2 \otimes \boldsymbol{I}_n\right). \end{aligned} \tag{62}$$

Based on (61), (48) is guaranteed if $\tilde{\boldsymbol{\Xi}} < 0$ and $\tilde{\boldsymbol{\Pi}} < 0$. We pre- and post multiply inequality $\tilde{\boldsymbol{\Xi}}$ by $\boldsymbol{T} = \mathrm{diag}(\boldsymbol{I}_{M-1} \otimes \boldsymbol{P}, \boldsymbol{I}_M \otimes \boldsymbol{P})$ which results in $\hat{\boldsymbol{\Xi}} = \begin{bmatrix} \hat{\boldsymbol{\Xi}}_{11} & \hat{\boldsymbol{\Xi}}_{12} \\ * & \hat{\boldsymbol{\Xi}}_{22} \end{bmatrix} < 0$, where

$$\begin{aligned} \hat{\boldsymbol{\Xi}}_{11} &= \boldsymbol{I}_{M-1} \otimes \left(\boldsymbol{P}\boldsymbol{A}^T + \boldsymbol{A}\boldsymbol{P}\right) + 2\tilde{\boldsymbol{J}}_1 \otimes \boldsymbol{B}\boldsymbol{K}_1 \boldsymbol{P} \\ &\quad + \tau_1^{-1}\left(\tilde{\boldsymbol{J}}_1 \otimes \boldsymbol{P}\right)^2 + 2\zeta_1 \boldsymbol{I}_{M-1} \otimes \boldsymbol{P} \\ \hat{\boldsymbol{\psi}}_{12} &= \tilde{\boldsymbol{J}}_1 \tilde{\boldsymbol{W}} \otimes \boldsymbol{B}\boldsymbol{K}_1 \boldsymbol{P} \\ \hat{\boldsymbol{\psi}}_{22} &= -\boldsymbol{I}_M \otimes \left(\boldsymbol{P}\boldsymbol{\Phi}_1^2 \boldsymbol{P}\right) + \tau_2^{-1} \boldsymbol{I}_M \otimes \boldsymbol{P}^2. \end{aligned} \tag{63}$$

Denote $\boldsymbol{\Omega} = \boldsymbol{K}_1 \boldsymbol{P}$ and $\tilde{\boldsymbol{\Phi}} = \boldsymbol{P}\boldsymbol{\Phi}_1^2 \boldsymbol{P}$ as alternative variables. Then, we apply the *Schur complement* Lemma [43] on $\hat{\boldsymbol{\Xi}}$ which results in $\boldsymbol{\Xi} < 0$ given in the statement of the theorem. Next, we denote $\tilde{\alpha} = \alpha_1^2$, $\tilde{\beta} = \beta_1^2$, $\tilde{\gamma} = \gamma_1$, and $\tilde{\rho} = \rho_1^2$. The following inequality is also considered:

$$-\tau_i^{-1} \le -2 + \tau_i, \qquad i \in \{1, 2\}. \tag{64}$$

Using $\tilde{\alpha}$, $\tilde{\beta}$, $\tilde{\gamma}$, $\tilde{\rho}$, and considering (64), inequalities $\pi_1 < 0$, $\pi_2 < 0$, and $\boldsymbol{\pi}_3 < 0$ given in the statement of the theorem are obtained. The relations between design parameters and decision variables are given in (30).

Motivated by [44, Sec. 2.2] and similar to [28], [45], a linear scalarization method is used to decrease/increase the decision variables used in $\boldsymbol{K}_1$, $\boldsymbol{\Phi}_1$, α_1, β_1, γ_1, and ρ_1 (see (30)). To this end, consider the following constraints:

$$\begin{aligned} &\boldsymbol{P}^{-1} < \theta_1 \boldsymbol{I} \quad \tilde{\boldsymbol{\Phi}}^T \tilde{\boldsymbol{\Phi}} < \theta_2 \boldsymbol{I} \quad \tilde{\alpha}^{-1} < \theta_3 \quad \tilde{\beta}^{-1} < \theta_4 \\ &\tilde{\gamma}^2 < \theta_5 \quad \tilde{\rho}^{-1} < \theta_6 \quad \boldsymbol{\Omega}^T \boldsymbol{\Omega} < \theta_7 \boldsymbol{I} \end{aligned} \tag{65}$$

where $\theta_c > 0$ $(1 \le c \le 7)$, are decision variables. Based on inequalities (65), if one decreases θ_c $(1 \le c \le 7)$, parameters $\{\|\tilde{\boldsymbol{\Phi}}\|, \tilde{\gamma}, \|\boldsymbol{\Omega}\|\}$ are decreased and parameters $\{\|\boldsymbol{P}\|, \tilde{\alpha}, \tilde{\beta}, \tilde{\rho}\}$ are increased. Therefore, design parameters $\{\|\boldsymbol{K}_1\|, \|\boldsymbol{\Phi}_1\|, \gamma_1\}$ are decreased and $\{\alpha_1, \beta_1, \rho_1\}$ are increased based on (30). These together increase MIET (25). Inequalities (32) are obtained from (65). The objective function $\mathbb{F}_1$ in (28) minimizes a weighted sum of the decision variables θ_c with all weights equal to 1. The LMIs given in (29) that include θ_c $(1 \le c \le 7)$, are equivalent to (65) using Schur complement. Once (28) is solved, design parameters are computed from (30). ■

APPENDIX B
PROOF OF THEOREM 3

Proof: The proof follows the same steps given in the proof of Theorem 2. Consider the following inequality:

$$\dot{V} + 2\zeta_2 V < 0 \tag{66}$$

where $V = V_1 + V_2$ with

$$V_1 = \tilde{\boldsymbol{\psi}}_{\mathcal{F}}^T \left(\boldsymbol{I}_N \otimes \boldsymbol{P}^{-1}\right) \tilde{\boldsymbol{\psi}}_{\mathcal{F}} \quad V_2 = \boldsymbol{\eta}_{\mathcal{F}}^T \boldsymbol{\eta}_{\mathcal{F}}. \tag{67}$$

From (23) and (67), it follows that:

$$\dot{V}_1 = \tilde{\boldsymbol{\psi}}_{\mathcal{F}}^T \bar{\boldsymbol{\Xi}}_{11} \tilde{\boldsymbol{\psi}}_{\mathcal{F}} + 2\tilde{\boldsymbol{\psi}}_{\mathcal{F}}^T \bar{\boldsymbol{\Xi}}_{12} \boldsymbol{e}_{\mathcal{F}} \tag{68}$$

where

$$\begin{aligned} \bar{\boldsymbol{\Xi}}_{11} &= \boldsymbol{I}_N \otimes (\boldsymbol{A}^T \boldsymbol{P}^{-1} + \boldsymbol{P}^{-1}\boldsymbol{A}) + 2\boldsymbol{J}_2 \otimes \boldsymbol{P}^{-1}\boldsymbol{B}\boldsymbol{K}_2 \\ \bar{\boldsymbol{\Xi}}_{12} &= \boldsymbol{J}_2 \boldsymbol{V}^{-1} \otimes \boldsymbol{P}^{-1}\boldsymbol{B}\boldsymbol{K}_2 \end{aligned} \tag{69}$$

In what follows, $\dot{V}_2$ is expanded based on (7):

$$\dot{V}_2 = 2\boldsymbol{\eta}_{\mathcal{F}}^T \left(-\gamma_2 \boldsymbol{\eta}_{\mathcal{F}} + \rho_2 \bar{\mathbb{X}}_{\mathcal{F}}\right). \tag{70}$$

Similar to (52) the following condition holds from (70):

$$\dot{V}_2 \leq (1 - 2\gamma_2)\, \boldsymbol{\eta}_{\mathcal{F}}^T \boldsymbol{\eta}_{\mathcal{F}} + \rho_2^2 \bar{\mathbb{X}}_{\mathcal{F}}^T \bar{\mathbb{X}}_{\mathcal{F}}. \tag{71}$$

The global form of (4) for followers is given below:

$$\mathbb{X}_{\mathcal{F}} = \boldsymbol{L}_{\mathcal{F}} \otimes \boldsymbol{I}_n \boldsymbol{\Lambda}_{\mathcal{F}} \hat{x}_{\mathcal{F}} + \boldsymbol{L}_{\mathcal{F}\mathcal{L}} \otimes \boldsymbol{I}_n \boldsymbol{x}_{\mathcal{L}}. \tag{72}$$

Considering $\boldsymbol{e}_{\mathcal{F}} = \boldsymbol{\Lambda}_{\mathcal{F}} \hat{x}_{\mathcal{F}} - \boldsymbol{x}_{\mathcal{F}}$, $\boldsymbol{V}\boldsymbol{J}_2\boldsymbol{V}^{-1} = \boldsymbol{L}_{\mathcal{F}}$, and transformation (17), we develop the following expression from (72):

$$\mathbb{X}_{\mathcal{F}} = \boldsymbol{\psi}_{\mathcal{F}} + (\boldsymbol{V}\boldsymbol{J}_2 \otimes \boldsymbol{I}_n)\boldsymbol{\sigma} \tag{73}$$

where $\boldsymbol{\sigma} = (\boldsymbol{V}^{-1} \otimes \boldsymbol{I}_n)\boldsymbol{e}_{\mathcal{F}}$. Recalling that $\boldsymbol{V}^T\boldsymbol{V} = \boldsymbol{I}$ (symmetric matrices have orthogonal eigenvectors), we expand $\bar{\mathbb{X}}_{\mathcal{F}}^T \bar{\mathbb{X}}_{\mathcal{F}}$

$$\bar{\mathbb{X}}_{\mathcal{F}}^T \bar{\mathbb{X}}_{\mathcal{F}} = \mathbb{X}_{\mathcal{F}}^T \mathbb{X}_{\mathcal{F}} = 2\boldsymbol{\psi}_{\mathcal{F}}^T \boldsymbol{\psi}_{\mathcal{F}} + 2\boldsymbol{\sigma}^T (\boldsymbol{J}_2 \otimes \boldsymbol{I}_n)^2 \boldsymbol{\sigma}. \tag{74}$$

The following upper-bound holds from (71) and (74):

$$\dot{V}_2 \leq (1 - 2\gamma_2)\, \boldsymbol{\eta}_{\mathcal{F}}^T \boldsymbol{\eta}_{\mathcal{F}} + 2\rho_2^2 \boldsymbol{\psi}_{\mathcal{F}}^T \boldsymbol{\psi}_{\mathcal{F}} + 2\rho_2^2 \boldsymbol{\sigma}^T (\boldsymbol{J}_2 \otimes \boldsymbol{I}_n)^2 \boldsymbol{\sigma}. \tag{75}$$

Based on (6), it holds that $\|\boldsymbol{\Phi}_2 \boldsymbol{e}_i(t)\| \leq \alpha_2 \|\mathbb{X}_i(t)\| + \beta_2 \eta_i(t)$. Let $\boldsymbol{a}_1 = [\|\boldsymbol{\Phi}_2 \boldsymbol{e}_1(t)\|, \ldots, \|\boldsymbol{\Phi}_2 \boldsymbol{e}_N(t)\|]^T$. Collectively, it holds that $\boldsymbol{a}_1 \leq \alpha_2 \bar{\mathbb{X}}_{\mathcal{F}} + \beta_2 \boldsymbol{\eta}_{\mathcal{F}}$, which is equivalent to

$$\begin{aligned} \boldsymbol{a}_1^T \boldsymbol{a}_1 = \boldsymbol{e}_{\mathcal{F}}^T \left(\boldsymbol{I}_N \otimes \boldsymbol{\Phi}_2^2\right) \boldsymbol{e}_{\mathcal{F}} &\leq \left(\alpha_2 \bar{\mathbb{X}}_{\mathcal{F}} + \beta_2 \boldsymbol{\eta}_{\mathcal{F}}\right)^T \left(\alpha_2 \bar{\mathbb{X}}_{\mathcal{F}} + \beta_2 \boldsymbol{\eta}_{\mathcal{F}}\right) \\ &\leq 2\alpha_2^2 \bar{\mathbb{X}}_{\mathcal{F}}^T \bar{\mathbb{X}}_{\mathcal{F}} + 2\beta_2^2 \boldsymbol{\eta}_{\mathcal{F}}^T \boldsymbol{\eta}_{\mathcal{F}}. \end{aligned} \tag{76}$$

Using (74), the following expression holds from (76):

$$\begin{aligned} \boldsymbol{e}_{\mathcal{F}}^T \left(\boldsymbol{I}_N \otimes \boldsymbol{\Phi}_2^2\right) \boldsymbol{e}_{\mathcal{F}} \leq & 4\alpha_2^2 \boldsymbol{\psi}_{\mathcal{F}}^T \boldsymbol{\psi}_{\mathcal{F}} + 4\alpha_2^2 \boldsymbol{\sigma}^T (\boldsymbol{J}_2 \otimes \boldsymbol{I}_n)^2 \boldsymbol{\sigma} \\ & + 2\beta_2^2 \boldsymbol{\eta}_{\mathcal{F}}^T \boldsymbol{\eta}_{\mathcal{F}}. \end{aligned} \tag{77}$$

The following equality holds by definition:

$$\tau_1^{-1} \left(\tilde{\boldsymbol{\psi}}_{\mathcal{F}}^T \tilde{\boldsymbol{\psi}}_{\mathcal{F}} - \boldsymbol{\psi}_{\mathcal{F}}^T \boldsymbol{\psi}_{\mathcal{F}}\right) = 0 \tag{78}$$

$$\tau_2^{-1} \left(\boldsymbol{e}_{\mathcal{F}}^T \boldsymbol{e}_{\mathcal{F}} - \boldsymbol{\sigma}^T \boldsymbol{\sigma}\right) \geq 0 \tag{79}$$

where $\tau_1 > 0$ and $\tau_2 > 0$ are decision variables. Let $\boldsymbol{\nu} = \left[\tilde{\boldsymbol{\psi}}_{\mathcal{F}}^T, \boldsymbol{e}_{\mathcal{F}}^T, \boldsymbol{\eta}_{\mathcal{F}}^T, \boldsymbol{\psi}_{\mathcal{F}}^T, \boldsymbol{\sigma}^T\right]^T$. Based on (68), (75), and (77)–(79), we re-arrange (66) as follows:

$$\boldsymbol{\nu}^T \begin{bmatrix} \tilde{\boldsymbol{\Xi}} & \boldsymbol{0} \\ * & \tilde{\boldsymbol{\Pi}} \end{bmatrix} \boldsymbol{\nu} < 0 \tag{80}$$

where $\tilde{\boldsymbol{\Xi}} = \begin{bmatrix} \tilde{\boldsymbol{\Xi}}_{11} & \bar{\boldsymbol{\Xi}}_{12} \\ * & \tilde{\boldsymbol{\Xi}}_{22} \end{bmatrix}$ and $\tilde{\boldsymbol{\Pi}} = \operatorname{diag}(\tilde{\boldsymbol{\pi}}_1, \tilde{\boldsymbol{\pi}}_2, \tilde{\boldsymbol{\pi}}_3)$ and

$$\begin{aligned} \tilde{\boldsymbol{\Xi}}_{11} &= \bar{\boldsymbol{\Xi}}_{11} + \tau_1^{-1} \boldsymbol{I}_{Nn} + 2\zeta_2 \boldsymbol{I}_N \otimes \boldsymbol{P}^{-1} \\ \tilde{\boldsymbol{\Xi}}_{22} &= -\boldsymbol{I}_N \otimes \boldsymbol{\Phi}_2^2 + \tau_2^{-1} \boldsymbol{I}_{Nn} \\ \tilde{\boldsymbol{\pi}}_1 &= \left(1 - 2\gamma_2 + 2\beta_2^2 + 2\zeta_2\right) \boldsymbol{I}_N \\ \tilde{\boldsymbol{\pi}}_2 &= \left(2\rho_2^2 - \tau_1^{-1} + 4\alpha_2^2\right) \boldsymbol{I}_{Nn} \\ \tilde{\boldsymbol{\pi}}_3 &= -\tau_2^{-1} \boldsymbol{I}_{Nn} + \left(4\alpha_2^2 + 2\rho_2^2\right) \left(\boldsymbol{J}_2^2 \otimes \boldsymbol{I}_n\right). \end{aligned} \tag{81}$$

Following the same steps given in (63)–(65) leads to the LMIs given in the statement of the Theorem. The proposed objective function (33) follows the same logic explained in Theorem 2 and that completes the proof. ■

REFERENCES

[1] Z. Wang, M. He, T. Zheng, Z. Fan, and G. Liu, "Guaranteed cost consensus for high-dimensional multi-agent systems with timevarying delays," *IEEE/CAA J. Autom. Sinica*, vol. 5, no. 1, pp. 181–189, 2017.

[2] W. Ni and D. Cheng, "Leader-following consensus of multi-agent systems under fixed and switching topologies," *Systems Control Lett.*, vol. 59, no. 3–4, pp. 209–217, 2010.

[3] A. Shariati and Q. Zhao, "Robust leader-following output regulation of uncertain multi-agent systems with time-varying delay," *IEEE/CAA J. Autom. Sinica*, vol. 5, no. 4, pp. 807–817, 2018.

[4] Z. Li, W. Ren, X. Liu, and M. Fu, "Distributed containment control of multi-agent systems with general linear dynamics in the presence of multiple leaders," *Int. J Robust Nonlin.*, vol. 23, no. 5, pp. 534–547, 2013.

[5] W. Liu, C. Yang, Y. Sun, and J. Qin, "Observer-based eventtriggered containment control of multi-agent systems with time delay," *Int. J. Systems Science*, vol. 48, no. 6, pp. 1217–1225, 2017.

[6] T.-H. Cheng, Z. Kan, J. R. Klotz, J. M. Shea, and W. E. Dixon, "Decentralized event-triggered control of networked systems part 2: Containment control, " in *Proc. IEEE American Control Conf.*, 2015, pp. 5444–5448.

[7] L. Ma, H. Min, S. Wang, Y. Liu, and Z. Liu, "Distributed containment control of networked nonlinear second-order systems with unknown parameters," *IEEE/CAA J. Autom. Sinica*, vol. 5, no. 1, pp. 232–239, 2016.

[8] A. Mondal, L. Behera, S. R. Sahoo, and A. Shukla, "A novel multi-agent formation control law with collision avoidance," *IEEE/CAA J. Autom. Sinica*, vol. 4, no. 3, pp. 558–568, 2017.

[9] X. Ge and Q.-L. Han, "Distributed formation control of networked multi-agent systems using a dynamic event-triggered communication mechanism," *IEEE Trans. Ind. Electron.*, vol. 64, no. 10, pp. 8118–8127, 2017.

[10] L. Han, X. Dong, Q. Li, and Z. Ren, "Formation-containment control for second-order multi-agent systems with time-varying delays," *Neurocomputing*, vol. 218, pp. 439–447, 2016.

[11] X. Dong, Y. Hua, Y. Zhou, Z. Ren, and Y. Zhong, "Theory and experiment on formation-containment control of multiple multirotor unmanned aerial vehicle systems," *IEEE Trans. Automation Science and Engineering*, vol. 16, no. 1, pp. 229–240, 2018.

[12] Y. Hua, X. Dong, L. Han, Q. Li, and Z. Ren, "Formationcontainment tracking for general linear multi-agent systems with a tracking-leader of unknown control input," *Systems & Control Letters*, vol. 122, pp. 67–76, 2018.

[13] Y.-W. Wang, X.-K. Liu, J.-W. Xiao, and Y. Shen, "Output formation-containment of interacted heterogeneous linear systems by distributed hybrid active control," *Automatica*, vol. 93, pp. 26–32, 2018.

[14] X. Dong, Q. Li, Z. Ren, and Y. Zhong, "Output formationcontainment analysis and design for general linear timeinvariant multi-agent systems," *J. Franklin I.*, vol. 353, no. 2, pp. 322–344, 2016.

[15] W. Jiang, G. Wen, Z. Peng, T. Huang, and R. A. Rahmani, "Fully distributed formation-containment control of heterogeneous linear multi-agent systems," *IEEE Trans. Automatic Control*, vol. 64, no. 9, pp. 3889–3896, 2019.

[16] S. Zuo, Y. Song, F. L. Lewis, and A. Davoudi, "Time-varying output formation containment of general linear homogeneous and heterogeneous multiagent systems," *IEEE Trans. Control of Network Systems*, vol. 6, no. 2, pp. 537–548, 2018.

[17] D. Li, W. Zhang, W. He, C. Li, and S. S. Ge, "Two-layer distributed formation-containment control of multiple euler-lagrange systems by output feedback," *IEEE Trans. Cybernetics*, vol. 49, no. 2, pp. 675–687, 2018.

[18] C. Li, L. Chen, Y. Guo, and G. Ma, "Formation-containment control for networked euler-lagrange systems with input saturation," *Nonlinear Dynamics*, vol. 91, no. 2, pp. 1307–1320, 2018.

[19] Y. Wang, Y. Song, and W. Ren, "Distributed adaptive finitetime approach for formation-containment control of networked nonlinear systems under directed topology," *IEEE Trans. Neural Networks and Learning Systems*, vol. 29, no. 7, pp. 3164–3175, 2017.

[20] L. Chen, C. Li, B. Xiao, and Y. Guo, "Formation-containment control of networked euler-lagrange systems: An event-triggered framework," *ISA Transactions*, vol. 86, pp. 87–97, 2019.

[21] L. Galbusera, G. Ferrari-Trecate, and R. Scattolini, "A hybrid model predictive control scheme for containment and distributed sensing in multi-agent systems," *Syst. Control Lett.*, vol. 62, no. 5, pp. 413–419, 2013.

[22] M. Yu, C. Yan, D. Xie, and G. Xie, "Event-triggered tracking consensus with packet losses and time-varying delays," *IEEE/CAA J. Autom. Sinica*, vol. 3, no. 2, pp. 165–173, 2016.

[23] H. Xia, W. X. Zheng, and J. Shao, "Event-triggered containment control for second-order multi-agent systems with sampled position data," *ISA Transactions*, 2017.

[24] G. Miao, J. Cao, A. Alsaedi, and F. E. Alsaadi, "Event-triggered containment control for multi-agent systems with constant time delays," *J. Franklin I.*, vol. 354, no. 15, pp. 6956–6977, 2017.

[25] W. Zou and Z. Xiang, "Event-triggered containment control of second-order nonlinear multi-agent systems," *J. Franklin Institute*, vol. 356, no. 17, pp. 10421–10438, 2019.

[26] W. Zou and Z. Xiang, "Event-triggered distributed containment control of heterogeneous linear multi-agent systems by an output regulation approach, " *Int. J. Systems Science*, vol. 48, no. 10, pp. 2041–2054, 2017.

[27] C. Peng and T. C. Yang, "Event-triggered communication and H_∞ control co-design for networked control systems," *Automatica*, vol. 49, no. 5, pp. 1326–1332, 2013.

[28] M. Abdelrahim, R. Postoyan, J. Daafouz, and D. Nešić, "Codesign of output feedback laws and event-triggering conditions for linear systems, " in *Proc. 53rd IEEE CDC*, 2014, pp. 3560–3565.

[29] W. Hu, C. Yang, T. Huang, and W. Gui, "A distributed dynamic event-triggered control approach to consensus of linear multiagent systems with directed networks," *IEEE Trans. Cybern.*, vol. 50, no. 2, pp. 869–874, 2020.

[30] X. Yi, K. Liu, D. V. Dimarogonas, and K. H. Johansson, "Dynamic event-triggered and self-triggered control for multi-agent systems," *IEEE Trans. Autom. Control*, vol. 64, no. 8, pp. 3300–3307, 2019.

[31] W. He, B. Xu, Q.-L. Han, and F. Qian, "Adaptive consensus control of linear multiagent systems with dynamic eventtriggered strategies," *IEEE Trans. Cybern.*, 2019.

[32] T.-H. Cheng, Z. Kan, J. R. Klotz, J. M. Shea, and W. E. Dixon, "Event-triggered control of multiagent systems for fixed and time-varying network topologies," *IEEE Trans. Autom. Control*, vol. 62, no. 10, pp. 5365–5371, 2017.

[33] L. Ding, Q.-L. Han, X. Ge, and X.-M. Zhang, "An overview of recent advances in event-triggered consensus of multiagent systems," *IEEE Trans. Cybern.*, vol. 48, no. 4, pp. 1110–1123, 2018.

[34] D. Yang, W. Ren, X. Liu, and W. Chen, "Decentralized eventtriggered consensus for linear multi-agent systems under general directed graphs," *Automatica*, vol. 69, pp. 242–249, 2016.

[35] G. S. Seyboth, D. V. Dimarogonas, and K. H. Johansson, "Event-based broadcasting for multi-agent average consensus," *Automatica*, vol. 49, no. 1, pp. 245–252, 2013.

[36] L. Xing, C. Wen, F. Guo, Z. Liu, and H. Su, "Event-based consensus for linear multiagent systems without continuous communication," *IEEE Trans. Cybern.*, vol. 47, no. 8, pp. 2132–2142, 2016.

[37] J. Almeida, C. Silvestre, and A. Pascoal, "Synchronization of multiagent systems using event-triggered and self-triggered broadcasts," *IEEE Trans. Autom. Control*, vol. 62, no. 9, pp. 4741–4746, 2017.

[38] X. Liu, C. Du, P. Lu, and D. Yang, "Distributed event-triggered feedback consensus control with state-dependent threshold for general linear multi-agent systems," *Int. J Robust Nonlin.*, vol. 27, no. 15, pp. 2589–2609, 2017.

[39] X. Dong, Q. Li, Q. Zhao, and Z. Ren, "Time-varying group formation analysis and design for general linear multi-agent systems with directed topologies," *Int. J. Robust and Nonlinear Control*, vol. 27, no. 9, pp. 1640–1652, 2017.

[40] A. Gusrialdi and Z. Qu, "Distributed estimation of all the eigenvalues and eigenvectors of matrices associated with strongly connected digraphs," *IEEE Contr. Syst. Lett.*, vol. 1, no. 2, pp. 328–333, 2017.

[41] I. Shames, T. Charalambous, C. N. Hadjicostis, and M. Johansson, "Distributed network size estimation and average degree estimation and control in networks isomorphic to directed graphs, " in *Proc. IEEE Communication, Control, and Computing (Allerton)*, 2012, pp. 1885–1892.

[42] J. R. Lawton, R. W. Beard, and B. J. Young, "A decentralized approach to formation maneuvers," *IEEE Trans. Robot. Autom.*, vol. 19, no. 6, pp. 933–941, 2003.

[43] S. Boyd, L. El Ghaoui, E. Feron, and V. Balakrishnan, *Linear Matrix Inequalities in System and Control Theory*. SIAM, 1994.

[44] G. Chiandussi, M. Codegone, S. Ferrero, and F. E. Varesio, "Comparison of multi-objective optimization methodologies for engineering applications," *Computers & Mathematics With Applications*, vol. 63, no. 5, pp. 912–942, 2012.

[45] M. Abdelrahim, R. Postoyan, J. Daafouz, D. Nešić, and M. Heemels, "Co-design of output feedback laws and eventtriggering conditions for

the L2-stabilization of linear systems," *Automatica*, vol. 87, pp. 337–344, 2018.

Amir Amini (S'16) received the B.Sc. degree from Shiraz University, Iran, in 2012. He received the M.Sc. degree from Tarbiat Modares University, Iran in 2015. He is currently a Ph.D. candidate in electrical and computer engineering at Concordia University, Canada. His research interests include distributed networked control systems, network optimization, and event-based strategies for control and estimation.

Amir Asif (M'97–SM'02) received the M.Sc. and Ph.D. degrees in electrical and computer engineering from Carnegie Mellon University (CMU), USA, in 1993 and 1996, respectively. He has been a Professor of electrical and computer engineering at Concordia University, Canada since 2014, where he is now serving as the Dean of the Faculty of Engineering and Computer Science. Previously, he was a Professor of electrical engineering and computer science at York University, Canada, from 2002 to 2014 and at the Faculty of CMU, where he was a Research Engineer from 1997 to 1999. He works in the area of statistical signal processing and communications. His current projects include error-resilient, scalable video compression; time-reversal, array imaging detection; genomic signal processing; and sparse, block-banded matrix technologies. He has authored over 150 technical contributions, including invited ones, published in international journals and conference proceedings, and a textbook "*Continuous and Discrete Time Signals and Systems*" published by the Cambridge University Press. He has served on the editorial boards of numerous journals and international conferences, including Associate Editor for *IEEE Transactions of Signal Processing* (2014–2018), *IEEE Signal Processing Letters* (2002–2006, 2009–2013). He has organized 4 IEEE conferences on signal processing theory and applications. He has received several distinguishing awards including the York University Faculty of Graduate Studies Teaching Award in 2008; York University Wide Teaching Award (Full-Time Senior Faculty Category) in 2008 from York University; the FSE Teaching Excellence Award (Senior Faculty Category) from York's Faculty of Science and Engineering in 2006 and in 2004; and the CSE Mildred Baptist Teaching Excellence Award from York's Department of Computer Science and Engineering in 2006 and in 2003. He is a Member of the Professional Engineering Society of Ontario.

Arash Mohammadi (S'08–M'14–SM'17) is an Assistant Professor with Concordia Institute for Information Systems Engineering (CIISE), Concordia University, Canada. He received the B.Sc. degree from University of Tehran, Iran, in 2005, the M.Sc. degree from Amirkabir University of Technology (Tehran Polytechnic), Iran, in 2007, and Ph.D. degree from York University, Canada in 2013. Prior to joining Concordia University and for 2 years, he was a Postdoctoral Fellow at Department of Electrical and Computer Engineering, University of Toronto, Canada. Dr. Mohammadi is currently the Director-Membership Developments of *IEEE Signal Processing Society* (SPS); Vice-Chair of *IEEE Signal Processing Montreal Chapter*, and Guest Editor for Special Issue entitled "Signal Processing for Neurorehabilitation and Assistive Technologies" at *IEEE Signal Processing Magazine*. He was the Organizing Committee Chair of "IEEE Signal Processing Society Winter School on Distributed Signal Processing for Secure Cyber-Physical Systems"; Co-Chair of the "*Symposium on Advanced Bio-Signal Processing and Machine Learning for Medical Cyber-Physical Systems*", as part of IEEE Global SIP'18; Lead Guest Editor for 2018 Special Issue entitled "Signal Processing for Security and Privacy in Networked Cyber-Physical Systems," at *IEEE Transactions on Signal & Information Processing Over Networks*, and Organizing Chair of *2018 IEEE Signal Processing Society Video & Image Processing (VIP) Cup*. Dr. Mohammadi has received several distinguishing awards, including the Eshrat Arjomandi Award for outstanding Ph.D. dissertation from Electrical Engineering and Computer Science Department of York University in 2013; Concordia President's Excellence in Teaching Award in 2018, and Both 2019 Gina Cody School of Engineering and Computer Science's Research and Teaching Awards in the new scholar category.